

United States Air Force Research Laboratory

Evaluation of the Effects of Variable Helmet Weight on Human Response During Lateral +Gy Impact

Chris E. Perry
John R. Buhrman

AIR FORCE RESEARCH LABORATORY

Erica J. Doczy
Stephen E. Mosher

GENERAL DYNAMICS, INC.
5200 Springfield Pke, Ste 200
Dayton OH 45431-1265

August 2003

Final Report for the Period August 1998 to February 1999

20040422 112

*Approved for public release; distribution
is unlimited.*

**Human Effectiveness Directorate
Biosciences & Protection Division
Biomechanics Branch**
2800 Q Street, BLdg 824, Rm 206
Wright-Patterson AFB OH 45433-7947

NOTICES

When US Government drawings, specifications, or other data are used for any purpose other than a definitely related Government procurement operation, the Government thereby incurs no responsibility nor any obligation whatsoever, and the fact that the Government may have formulated, furnished, or in any way supplied the said drawings, specifications, or other data, is not to be regarded by implication or otherwise, as in any manner licensing the holder or any other person or corporation, or conveying any rights or permission to manufacture, use, or sell any patented invention that may in any way be related thereto.

Please do not request copies of this report from the Air Force Research Laboratory. Additional copies may be purchased from:

National Technical Information Service
5285 Port Royal Road
Springfield, Virginia 22161

Federal Government agencies registered with the Defense Technical Information Center should direct requests for copies of this report to:

Defense Technical Information Center
8725 John J. Kingman Rd., Ste 0944
Ft. Belvoir VA 22060-6218

The voluntary informed consent of the subjects used in this research was obtained as required by Air Force Instruction 40-402.

DISCLAIMER

This Technical Report is published as received and has not been edited by the Technical Editing Staff of the Air Force Research Laboratory.

TECHNICAL REVIEW AND APPROVAL

AFRL-HE-WP-TR-2004-0013

This report has been reviewed by the Office of Public Affairs (PA) and is releasable to the National Technical Information Service (NTIS). At NTIS, it will be available to the general public, including foreign nations.

This technical report has been reviewed and is approved for publication.

FOR THE DIRECTOR

//Signed//

THOMAS L. CROPPER, Col, USAF
Chief, Biosciences and Protection Division
Air Force Research Laboratory

REPORT DOCUMENTATION PAGE					Form Approved OMB No. 0704-0188	
The public reporting burden for this collection of information is estimated to average 1 hour per response, including the time for reviewing instructions, searching existing data sources, gathering and maintaining the data needed, and completing and reviewing the collection of information. Send comments regarding this burden estimate or any other aspect of this collection of information, including suggestions for reducing the burden, to Department of Defense, Washington Headquarters Services, Directorate for Information Operations and Reports (0704-0188), 1215 Jefferson Davis Highway, Suite 1204, Arlington, VA 22202-4302. Respondents should be aware that notwithstanding any other provision of law, no person shall be subject to any penalty for failing to comply with a collection of information if it does not display a currently valid OMB control number.						
PLEASE DO NOT RETURN YOUR FORM TO THE ABOVE ADDRESS.						
1. REPORT DATE (DD-MM-YYYY) Aug 2003		2. REPORT TYPE Final			3. DATES COVERED (From - To) August 1998 to February 1999	
4. TITLE AND SUBTITLE Evaluation of the Effects of Variable Helmet Weight on Human Response During Lateral +Gy Impact				5a. CONTRACT NUMBER		
				5b. GRANT NUMBER		
				5c. PROGRAM ELEMENT NUMBER 62202F		
				5d. PROJECT NUMBER 7184		
6. AUTHOR(S) Chris E. Perry, John R. Buhrman (AFRL/HEPA) Erica J. Doczy, Stephen E. Mosher (General Dynamics)				5e. TASK NUMBER 02		
				5f. WORK UNIT NUMBER 71840201		
7. PERFORMING ORGANIZATION NAME(S) AND ADDRESS(ES) Air Force Research Laboratory, Human Effectiveness Directorate Biosciences and Protection Division Biomechanics Branch Air Force Materiel Command Wright-Patterson AFB OH 45433-7947					8. PERFORMING ORGANIZATION REPORT NUMBER AFRL-HE-WP-TR-2004-0013	
9. SPONSORING/MONITORING AGENCY NAME(S) AND ADDRESS(ES)					10. SPONSOR/MONITOR'S ACRONYM(S)	
					11. SPONSOR/MONITOR'S REPORT NUMBER(S)	
12. DISTRIBUTION/AVAILABILITY STATEMENT Approved for public release; distribution is unlimited						
13. SUPPLEMENTARY NOTES						
14. ABSTRACT Helmet-mounted systems (HMS) are designed to enhance pilot performance, but may also affect pilot safety by increasing the potential for neck injury during ejection due to the change in helmet inertial properties. A series of tests was conducted by AFRL/HEPA on a horizontal impulse accelerator using human subjects to investigate the effects of helmet inertial properties on human response to short duration sideward impacts of variable magnitude. The effects of headrest contour and gender were also investigated. Maximum neck load values obtained in this study will be used to establish head/neck injury criteria for helmet-mounted systems and for the implementation of improvements in bracing techniques to minimize pilot injury during ejections.						
15. SUBJECT TERMS Helmet Mounted Systems, Impact Acceleration, Helmet Weight, Ejection Injury, Gender Acceleration Effects, Pilot Bracing, Headrest Properties						
16. SECURITY CLASSIFICATION OF:			17. LIMITATION OF ABSTRACT UL	18. NUMBER OF PAGES 81	19a. NAME OF RESPONSIBLE PERSON John R. Buhrman	
a. REPORT UC	b. ABSTRACT UC	c. THIS PAGE UC			19b. TELEPHONE NUMBER (Include area code) (937) 255-3121	

THIS PAGE LEFT BLANK INTENTIONALLY

PREFACE

The impact tests and data analysis described in this report were accomplished by the Biomechanics Branch, Human Effectiveness Directorate of the Air Force Research Laboratory (AFRL/HEPA) at Wright-Patterson Air Force Base, Ohio. The test facility for this study was the Horizontal Impulse Accelerator (HIA). Engineering support at AFRL/HEPA was provided by DynCorp under contract F3301-96-DJ001.

This page intentionally left blank.

TABLE OF CONTENTS

	Page No.
INTRODUCTION.....	1
BACKGROUND	1
METHODS	2
RESULTS	7
DISCUSSION	25
CONCLUSIONS.....	27
REFERENCES	29
APPENDIX A. Test Configuration and Data Acquisition System	31
APPENDIX B. Subject Anthropometry/ Instrumentation Channel Definitions	55
APPENDIX C. Sample Acceleration/Force Data	59

LIST OF TABLES

Table	Page No.
1 Gy Impact Test Matrix	2
2 Summary of Subject Anthropometry Averages	4
3 General Acceleration Summary	7
4 Human Head Acceleration Response Summary	8
5 Human Neck Load and Moment Response Summary	11
6 Summary of Mean Peak Headrest Forces	13
7 Gender Comparison of Y Loads and Moments	14
8 Summary of Mean Displacement Data	20
9 Gender Comparison of Resultant Displacements at Helmet Top/Forehead.....	23

LIST OF FIGURES

Figure		Page No.
1	Air Force Research Laboratory Horizontal Impulse Accelerator.....	3
2	Front and Side Views of Test Setup Showing Seat and Initial Position	4
3	Anatomical Axis System of the Human Head	5
4	General Acceleration Summary as a Function of Sled Acceleration	7
5	Human Head X and Y Linear Acceleration Response Summary as a Function of Sled Acceleration.....	9
6	Human Head Y and Z Angular Acceleration Response Summary as a Function of Sled Acceleration.....	9
7	Human Head X and Y Linear Acceleration Response Summary as a Function of Helmet Weight	10
8	Human Head Y and Z Angular Acceleration Response Summary as a Function of Helmet Weight	10
9	X and Y Neck Load Response Summary and Extrapolation as a Function of Increasing Sled Acceleration	11
10	Y and Z Neck Moment Response Summary and Extrapolation as a Function of Increasing Sled Acceleration	12
11	X and Y Neck Load Response Summary as a Function of Helmet Weight.....	12
12	Y and Z Neck Moment Response Summary as a Function of Helmet Weight.....	13
13	Gender Comparison of X and Y Neck Loads as a Function of Sled Acceleration	14
14	Gender Comparison of Y and Z Neck Moments as a Function of Sled Acceleration	15
15	Gender Comparison of X and Y Neck Loads as a Function of Helmet Weight	15
16	Gender Comparison of Y and Z Neck Moments as a Function of Helmet Weight	16
17	Peak Load Comparison of Contoured Vs. Flat Headrest	16
18	Summary of Pre-Impact Headrest Forces as a Function of Sled Acceleration	17
19	Summary of Pre-Impact Headrest Forces as a Function of Helmet Weight	17
20	Gender Comparison of Pre-Impact Headrest Forces as a Function of Sled Acceleration	18
21	Gender Comparison of Pre-Impact Headrest Forces as a Function of Helmet Weight	19
22	Summary of Peak X Displacement as a Function of Sled Acceleration	20
23	Summary of Peak Y Displacement as a Function of Sled Acceleration	21
24	Summary of Peak Z Displacement as a Function of Sled Acceleration.....	21

25	Summary of Peak X Displacement as a Function of Helmet Weight	22
26	Summary of Peak Y Displacement as a Function of Helmet Weight	22
27	Summary of Peak Z Displacement as a Function of Helmet Weight.....	23
28	Gender Comparison of Peak Resultant Displacement as a Function of Sled Acceleration	24
29	Gender Comparison of Peak Resultant Displacement as a Function of Helmet Weight	24
30	Peak Displacement Comparison of Contoured Vs. Flat Headrest	25

INTRODUCTION

Helmet-mounted systems (HMS), such as night vision goggles and helmet-mounted displays, are designed to enhance pilot performance through improvements in situational awareness, target acquisition, and weapon delivery. However, using HMS may also affect pilot safety by increasing the potential for neck injury during all phases of ejection (catapult stroke, windblast, seat stabilization, parachute opening-shock). This increased neck injury potential is due to the increase in dynamic forces generated in the cervical spine as a result of the change in helmet inertial properties including weight, center-of-gravity (Cg), and moments-of-inertia (MOI). Research is therefore required to establish the relationship between helmet inertial properties and human impact response in the three coordinate axes. Test results could then be used to define acceptable helmet inertial properties for the ejection environment.

A series of tests were conducted by AFRL/HEPA to investigate the effects of helmet inertial properties on human response to short-duration sideward (+Gy) impacts of variable magnitude. This study provided dynamic human head response data (acceleration and motion analysis) not collected in a previous AFRL sideward impact test program.

BACKGROUND

Tests by Perry at the Air Force Research Lab's Biodynamics and Acceleration Branch (AFRL/HEPA) from 1991 through 1997 evaluated the effects of variable helmet inertial properties on the biodynamic response of male and female human volunteers exposed to vertical (+Gz) impact accelerations using the Vertical Deceleration Tower (VDT) [1, 6-11]. Over 600 vertical impacts were conducted to develop a relationship between human dynamic response and helmet inertial properties. The volunteers were exposed to vertical impact accelerations at a maximum peak impact level of 10 G with pulse duration of approximately 150 ms, and with a maximum total head-supported weight of 7.0 lbs. Measured chest accelerations were used as an input to a computer model to calculate dynamic head accelerations relative to the head anatomical center-of-gravity and neck loads generated at the occipital condyles. In 1992 and 1993, an investigation of the human response to varied +Gy impact duration and magnitude was conducted by Strzelecki using the Horizontal Impulse Accelerator (HIA) [12]. Over 240 +Gy impact tests with human volunteers were conducted at peak acceleration levels ranging from 4 to 7 G and at pulse durations ranging from 31 to 250 ms. Test subjects wore a standard USAF helmet for all test conditions. Data from this study were used for the evaluation of whole-body response.

Additional dynamic data from a +Gy impact environment with variable helmet weight were required to continue the development of a human biodynamic response database for the three coordinate axes and to continue the development of human biodynamic response models. This experimental study was conducted to evaluate the effects of helmet inertial properties on human biodynamic response during sideward impact. The results will provide critical information to the developers of advanced biodynamics computer models and to designers of helmet-mounted systems. The test program maximized information with minimal injury potential due to the sub-

injury level impact exposures. Tests were conducted at peak acceleration levels ranging from 4 to 6 G, with a pulse duration of approximately 150 ms. Total head-supported weight varied from 0 to 4.5 lbs.

METHODS

A series of short-duration sideward impact acceleration tests were conducted with male and female volunteer subjects using the HIA. The study was conducted to evaluate the effects of variable helmet inertial properties and impact acceleration magnitudes on subject head and torso displacements and accelerations. To accomplish this, the acceleration magnitude and helmet inertial property experimental conditions were varied. The sideward acceleration profile generated by the HIA approximated a half-sine pulse with rise-time of 75 ms and pulse duration of 150 ms. The peak of the impact pulse was varied in magnitude from 4 to 6 G. These values had been previously tested, and were well tolerated by the volunteer human subjects [12]. Prior to human testing, three tests were conducted in each condition with an instrumented, large Advanced Dynamic Anthropomorphic Manikin (ADAM). The experimental test matrix is shown in Table 1.

Table 1. Gy Impact Test Matrix

Test Cell	Sled Acceleration Level (G)	Head-Supported Weight (lbs)	Headrest
A	4	3.0	Contoured
B	5	3.0	Contoured
C	6	3.0	Contoured
D	5	0.0	Flat
E	5	0.0	Contoured
F	5	4.5	Contoured

All tests were conducted using the AFRL/HEPA HIA facility located in Bldg. 824, Area B, Wright-Patterson AFB OH. The HIA consists of a 4 x 8 foot sled positioned on a 240-foot long track, and a 24-inch diameter pneumatic actuator. The HIA operates on the principle of differential gas pressures acting on both surfaces of a thrust piston in a closed cylinder. The impact acceleration occurs at the beginning of the experiment as stored high-pressure air is allowed to impinge on the surface of the thrust piston thus propelling the sled. As the sled breaks contact with the thrust piston, the sled coasts to a stop or is stopped with a pneumatic brake system. Pulses in the \pm Y-axis of the test subject can be produced by rotating the seat/test fixture 90 degrees relative to the length of the track and the long edge of the sled. A photo of the HIA is shown in Figure 1. For more information on this facility, refer to Appendix A.

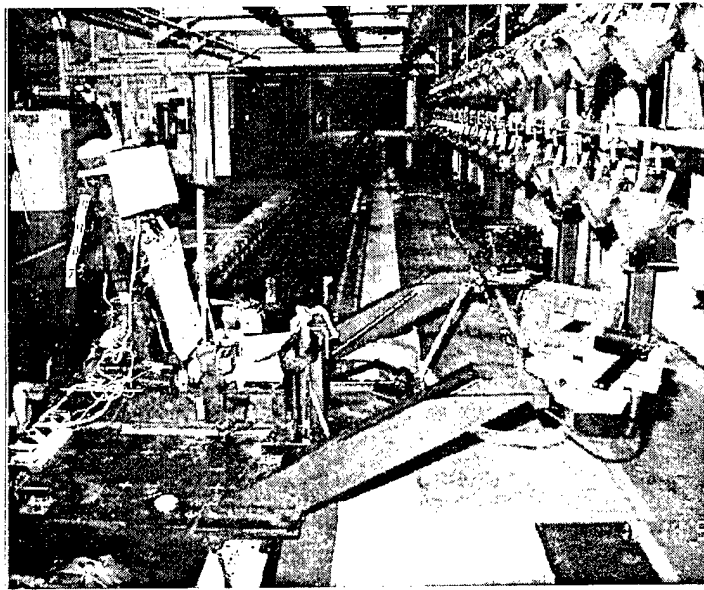


Figure 1. Air Force Research Laboratory Horizontal Impulse Accelerator

All tests were conducted using the "40 G Seat" mounted on the HIA sled. The seat was mounted such that the input acceleration pulse was applied across the chest of the subject (sideward or lateral impact). All subjects (human and manikin) were seated in an upright posture and restrained to the seat. The set-up of this study is shown in Figure 2. For Cells A, B, C, E, and F, the seat used a contoured headrest with side extension to prevent excessive neck twisting and to prevent the head from traveling behind the headrest following impact. A flat headrest was used for Cell D. The headrests were in-line with the seat back. The seat back was perpendicular to the seat pan, and the seat pan was reclined approximately 13° from the horizontal plane of the sled. All subjects were fitted with a PCU-15/P torso harness prior to being positioned in the seat.

Each subject also wore a standard HBU lap belt. The restraint straps were pre-tensioned at the shoulders and the lap attachment points to 20 ± 5 lbs prior to each test. The subject's feet were individually restrained using Velcro straps attached to the footrests. The subject's hands were positioned under Velcro thigh straps. Padded support plates were located at the right thigh/hip and at each knee with the plates positioned on the right side of the knee.

BEST AVAILABLE COPY

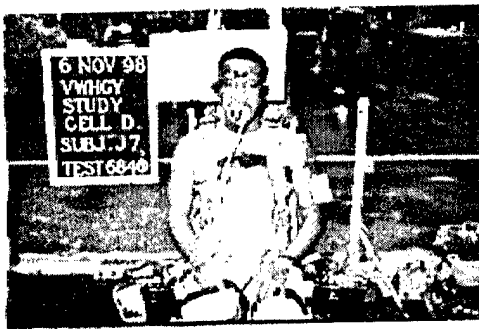


Figure 2. Front and Side Views of Test Setup Showing Seat Fixture with Flat and Contoured Headrests and Subject Initial Position

The Variable Weight Impact (VWI) helmet consisted of a modified HGU-55/P flight helmet (size L) with identical weights placed on each side of the helmet to maintain symmetry. The VWI was used successfully in previous tests by Perry [1, 6-11]. The interior volume of the helmet was adjusted for the test subjects whose heads did not fit into a large size helmet (determined using head length and breadth dimensions). This was accomplished by using helmet space pads located at the crown, behind each ear cup, and at the rear of the helmet.

The subject population consisted of the large ADAM (manikin), and 21 male and 10 female volunteer subjects. All human subjects were members of AFRL/HE Impact Acceleration Test Panel. Each subject had completed a series of individual anthropometric measurements prior to participation in the test program (Appendix B). The average characteristics of the subject sample are summarized in Table 2. This test program was formally approved by the Wright Research Site Institutional Review Board (WRS IRB) under protocol 98-03 [5].

Table 2. Summary of Subject Anthropometry Averages

	Age (yr)	Weight (lbs)	Standing Ht. (in)	Sitting Ht. (in)
ADAM	N/A	218	73.6	38.7
Males	32.9 ± 6.0	192.0 ± 28.5	70.0 ± 2.1	36.8 ± 1.3
Females	27.5 ± 4.3	145.3 ± 16.8	65.1 ± 1.4	34.5 ± 0.9
All Human Subjects	31.1 ± 6.0	177.0 ± 33.5	68.4 ± 3.0	36.0 ± 1.6

The pre-impact position of the subjects was documented with still photographs before each test. Motion analysis data were collected for all tests starting 2-3 seconds prior to sled impact. These data were collected using two Selspot infrared detection cameras that recorded the position of 10 infrared markers (4 mounted on the test fixture and 6 mounted on the test subject) at 500 samples per second. Processed Selspot data consisted of relative displacement curves, and displacement and velocity time histories. In addition to the Selspot cameras, a single Kodak high-speed video camera operating at 1000 frames per second was also secured to the sled camera mount and was used for visual documentation of the impact event. For more information on the Selspot motion analysis system and video system, refer to Appendix A.

Measured electronic data included sled velocity and accelerations, seat accelerations, subject head and torso accelerations and displacements, and forces developed in the seat and the restraint system. Shown in Figure 3 is the head anatomical axis system referenced in this study. A positive Y moment is represented by forward flexion. The head accelerations were measured with a triaxial accelerometer array mounted on a bite bar. A second triaxial accelerometer array was positioned at the subject's chest with a Velcro chest strap. An x and y-axis accelerometer package was placed at T1. The bite bar accelerometer array also contained two angular accelerometers to record rotational acceleration about the y-axis and the z-axis. Triaxial accelerometer packages were also used to record seat pan and sled accelerations. Load cells were used to measure the forces generated at the seat pan, headrest, and lap and shoulder strap attachment points. For details on the instrumentation, refer to Appendix A.

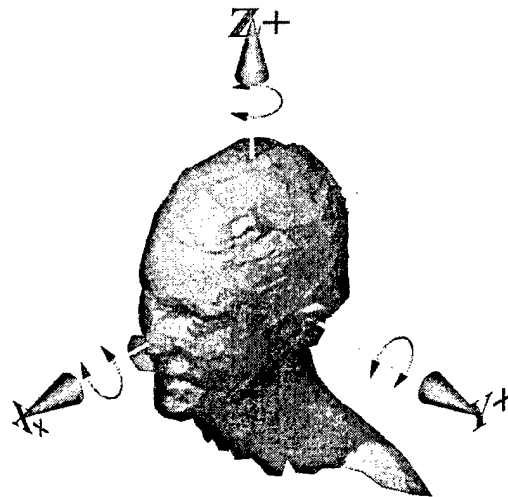


Figure 3. Anatomical Axis System of the Human Head.

All test data were organized in individual test data files containing channel time histories, peak and time-to-peak analysis, and summary plots. In the peak value analysis, a time frame of 200 ms was used to omit from the evaluation the acceleration peaks due to headrest strikes following rebound. Each test cell had its corresponding data organized into a file containing simple summary statistics (mean and standard deviation) on the measured and calculated parameters. One test cell file was designated for the maximum values and one file for the minimum values. The statistical analyses were performed on the data using Microsoft® Excel 2002 and ProStat Version 2.5, both commercially available software packages.

Prior to statistical analysis of the test acceleration data, an evaluation was performed on each set of data per cell to search for outliers using the Grubb's Test [13]. The Grubb's Test generates a range that the data can be expected to cover within a specific confidence level. The data limits of the range are generated using the following equations:

$$\begin{aligned}\text{Upper Limit} &= \bar{x} + T \cdot s \\ \text{Lower Limit} &= \bar{x} - T \cdot s\end{aligned}$$

where \bar{x} is the data set mean, s is the sample standard deviation, and T is the critical Grubb's T -value which is dependent on the sample size and confidence level. For this evaluation a 95% confidence level was used. A total of fifteen tests were removed due to outliers found within the 200 ms window of interest in the Head X, Y, Ry and Rz acceleration peaks.

To evaluate head and torso displacement, accelerations, and forces as a function of variable inertial properties and acceleration magnitudes, cells A, B, C, E, and F were examined (all contoured headrests). The measured headrest pre-impact loads were also statistically evaluated for these cells. The headrest pre-impact load is the magnitude of force applied to the headrest by the subject just prior to impact as a result of required bracing techniques. A pre-impact headrest load average was taken from the loads that were recorded over a 25 ms time frame before impact at a sample rate of 1000 Hz. The purpose of this evaluation was to observe the effect of the subject's knowledge of the impending sled acceleration on how forcefully the subject placed his or her head against the headrest.

The human subjects' neck loads and moments were calculated using measured head acceleration data. An in-house program, "Neckload3," used the head accelerations (collected with the bite bar instrumentation package) and the inertial properties of the head/helmet to approximate the loads and moments seen at the occipital condyle (head-neck joint or OC). The inertial properties were approximated by a sub-routine of "Neckload3" called "Combine." "Combine" approximates the inertial properties of the subject's head with helmet using the subject's total body weight, head circumference, and previously measured helmet inertial properties. Because "Neckload3" does not take into account external loads on the head, the program output represents the loads and torques after the head has separated from the headrest. "Neckload3" generated a per-test output data file in Excel containing the load and torque time histories, neck load summary sheet, Neck Injury Criteria (Nij) time history, and Nij summary sheet. Nij is a linear combination of tension/compression and flexion/extension moments used to help determine probability of injury of the neck [3]. Again, a time frame of 200ms was used to omit the rebound effect from the evaluation. The in-house program, "NeckloadDb," used the summary sheets of each test to create a neck load database for maximum and minimum values within each cell.

For each test, a Selspot time history Excel file was created. The files contained displacement data for the chest, left temple, right temple, helmet top (forehead when no helmet was used), and mouth. The peak displacements for the helmet top and mouth were examined using the time frame of 200 ms. An in-house program, "UpdateExtremaSelspot," was used to create a Selspot database for the maximum and minimum values within each cell. Simple statistics were employed to calculate the mean and standard deviation for each measurement within all cells.

The head displacements, accelerations, and forces were examined for significant differences among varying test parameters, including head-supported weights, different acceleration magnitudes, and between male and female subjects. In this study, the linear X, linear Y, angular Y, and angular Z acceleration and corresponding force parameters were of particular interest. Cell D (flat headrest) was evaluated and compared to Cell E (contoured headrest) to determine the effects, if any, that the headrest had on head displacement and neck loads. Both these cells were conducted at a peak sled acceleration of 5 G with the subject wearing no helmet.

RESULTS

Acceleration Response: A total of 176 tests were evaluated following outlier removal. The sled, seat, and chest acceleration responses in the direction of impact are shown in Table 3 and plotted in Figure 4. The mean and standard deviation are identified for each parameter in each of the six test conditions. The small standard deviation values of the sled acceleration indicate excellent control of the sled parameters. The maximum mean peak chest acceleration was 9.84 G at a sled acceleration of 5.99 G. The ratio of chest acceleration to input (sled) acceleration was approximately 1.6:1. The mean peak values of the seat acceleration were slightly higher than the mean sled acceleration due to small vibrations in the seat.

Table 3. General Acceleration Summary

Test Cell	Sled Accel (G)	Seat Y Accel (G)	Chest Y Accel (G)
A	4.05 ± 0.09	4.49 ± 0.14	6.40 ± 0.48
B	5.02 ± 0.05	5.50 ± 0.18	8.29 ± 0.97
C	5.99 ± 0.06	6.54 ± 0.17	9.84 ± 1.01
D	5.02 ± 0.06	5.55 ± 0.16	8.87 ± 1.01
E	5.02 ± 0.06	5.53 ± 0.16	7.82 ± 0.68
F	4.97 ± 0.07	5.49 ± 0.17	7.33 ± 0.46

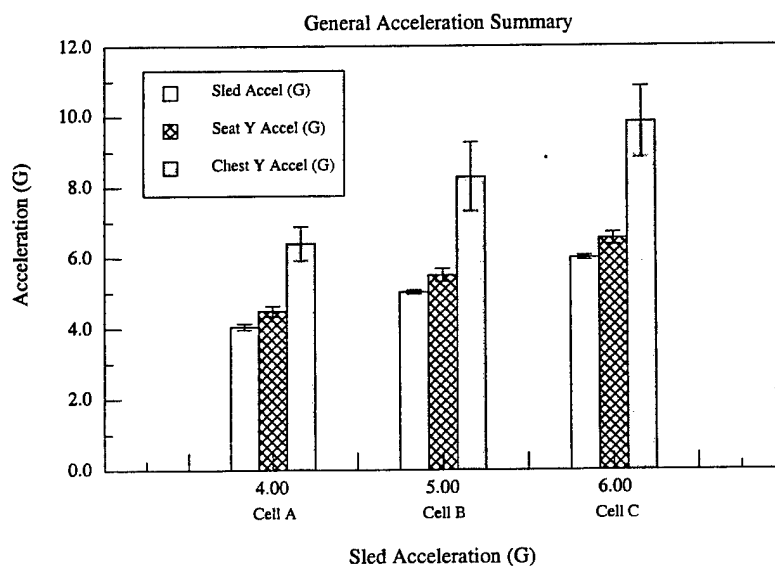


Figure 4. General Acceleration Summary as a Function of Sled Acceleration

The results from the statistical evaluation of the pertinent head acceleration response parameters are shown in Table 4. The peak Y acceleration was in the direction of the impact, from right to left. The peak X acceleration was in the direction normal to the impact vector, toward the back of the head. The prominent Y angular acceleration (pitch) of the head occurred in flexion (positive Y moment). These accelerations were plotted against both increasing sled acceleration level and helmet weight, shown in Figures 5-8. The mean peak head Ry acceleration decreased 5.3% as the sled acceleration increased from 5 G to 6 G. All other measured accelerations increased with increasing G level. As head-supported weight increased from 0.0 lbs (cell E) to 3.0 lbs (cell B), all head accelerations increased. As helmet weight increased from 3.0 lbs (cell B) to 4.5 lbs (cell F), all head accelerations decreased. An 11.6% decrease in mean peak head Y accelerations was observed in cell F as compared to cell B (statistically significant at $\alpha = 0.05$).

Table 4. Human Head Acceleration Response Summary

Test Cell	Sled Accel (G)	Head X Accel (G)	Head Y Accel (G)	Head Ry (Rad/Sec ²)	Head Rz (Rad/Sec ²)
A	4.05 ± 0.09	4.42 ± 1.41	6.82 ± 1.20	265.88 ± 199.76	364.17 ± 110.81
B	5.02 ± 0.05	6.04 ± 1.66	8.72 ± 1.25	359.69 ± 281.82	473.41 ± 204.51
C	5.99 ± 0.06	6.96 ± 1.85	10.67 ± 1.83	340.51 ± 131.80	562.05 ± 336.65
D	5.02 ± 0.06	3.11 ± 1.01	8.20 ± 1.21	212.09 ± 74.54	395.37 ± 118.65
E	5.02 ± 0.06	5.44 ± 1.20	7.86 ± 0.95	302.36 ± 95.96	443.87 ± 96.84
F	4.97 ± 0.07	4.73 ± 0.73	7.71 ± 1.09	245.91 ± 93.83	331.97 ± 95.38

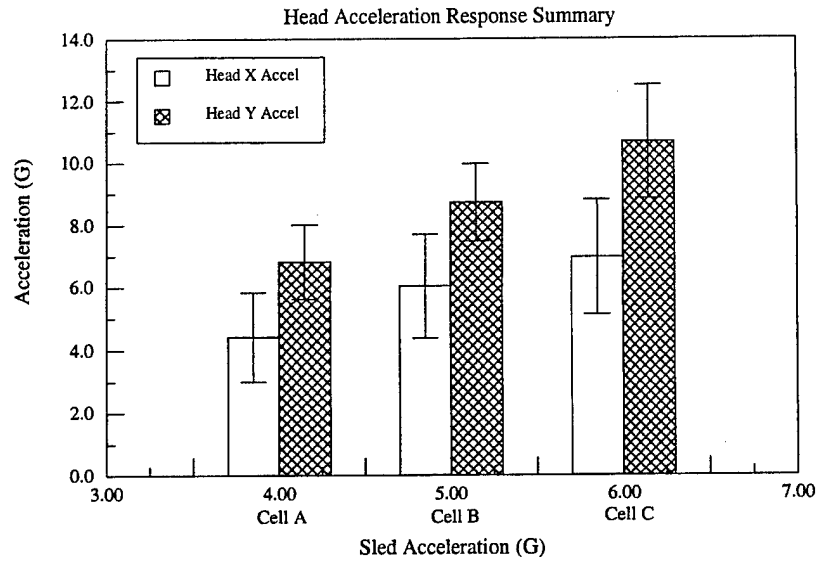


Figure 5. Human Head X and Y Linear Acceleration Response Summary as a Function of Sled Acceleration

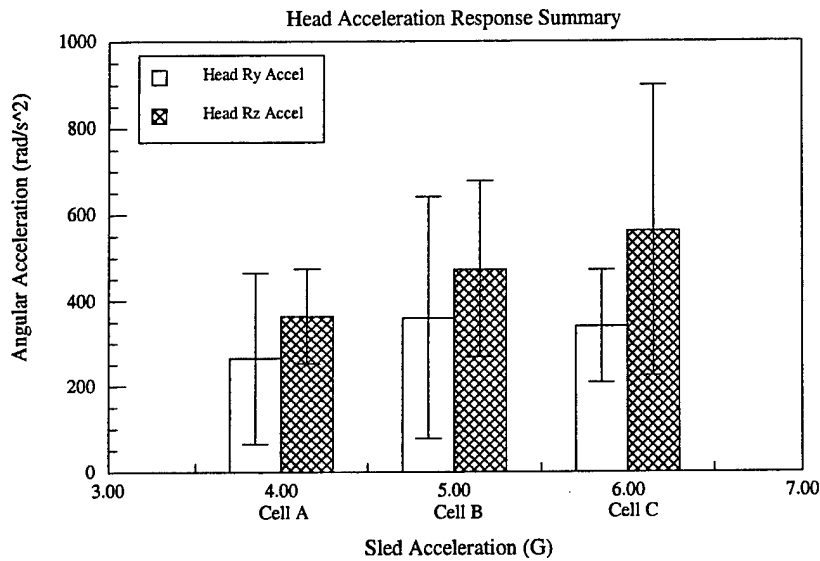


Figure 6. Human Head Y and Z Angular Acceleration Response Summary as a Function of Sled Acceleration

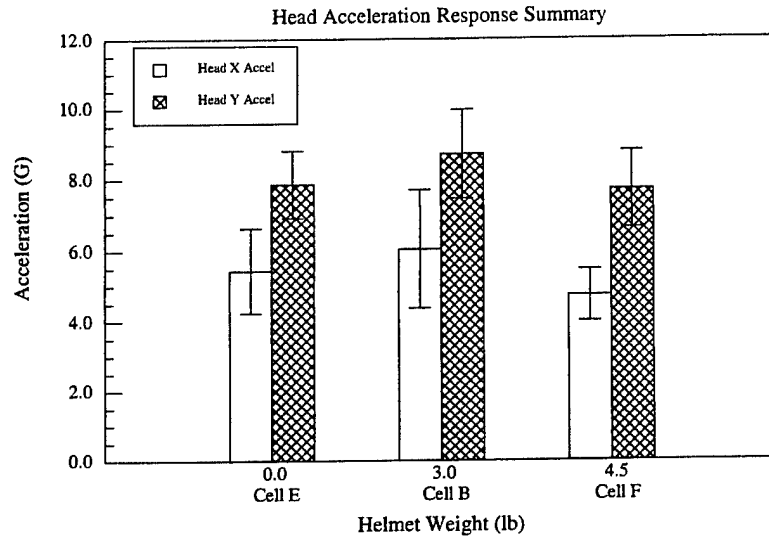


Figure 7. Human Head X and Y Linear Acceleration Response Summary as a Function of Helmet Weight

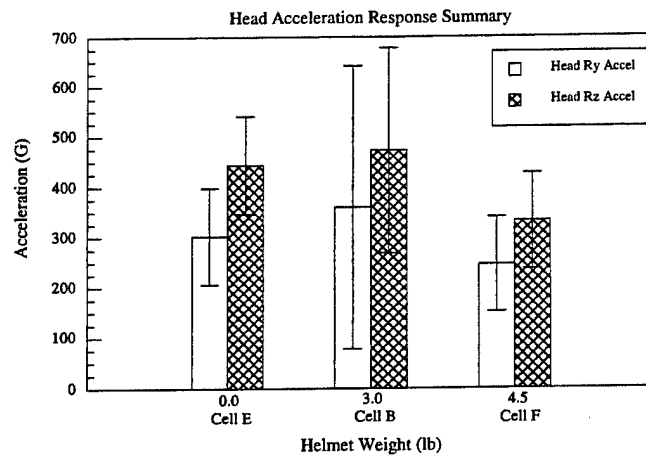


Figure 8. Human Head Y and Z Angular Acceleration Response Summary as a Function of Helmet Weight

Neck Loads and Moments: The mean peak estimated neck loads and moments are listed in Table 5. These loads and moments were plotted against both increasing sled acceleration level and helmet weight, and are shown in Figures 9-12. The X and Y neck loads (shear loads) and Y and Z moments (rotational torques) all increased with increasing G level. Also shown in Figures 9 and 10 are extrapolations for the neck loads and moments up to a sled acceleration of 10 G. These extrapolations indicate that at a sled acceleration of 10 G and assuming a linear increase in response, the human neck would experience an X load of 168 lbs, Y load of 389 lbs, Y moment of 411 in-lbs, and Z moment of 231 in-lbs. All loads and moments (except Head Mz) increased when the 3.0 lb helmet was added (cell B) compared to the no-helmet condition (cell E). When

the helmet weight was increased to 4.5 lbs (cell F), small decreases in all loads and moments were observed as compared to the 3.0 lb helmet condition (Cell B). This included Y force that decreased 6.9% (not significant at $\alpha = 0.05$) and Mz that decreased 15.2% (significant at $\alpha = 0.05$).

Table 5. Human Neck Load and Moment Response Summary

Test Cell	Head X Load (lbs)	Head Y Load (lbs)	Head My (in-lbs)	Head Mz (in-lbs)
A	50.72 ± 11.63	142.92 ± 35.18	156.19 ± 59.98	62.58 ± 20.86
B	70.78 ± 17.90	185.47 ± 34.37	198.40 ± 74.37	87.63 ± 16.86
C	89.79 ± 27.59	224.69 ± 59.24	241.05 ± 92.10	118.98 ± 32.96
D	42.89 ± 14.93	129.26 ± 32.66	130.53 ± 55.75	121.62 ± 27.13
E	56.97 ± 7.18	135.74 ± 22.81	155.28 ± 25.74	117.52 ± 20.04
F	66.00 ± 9.37	172.64 ± 31.14	173.18 ± 43.06	74.28 ± 17.45

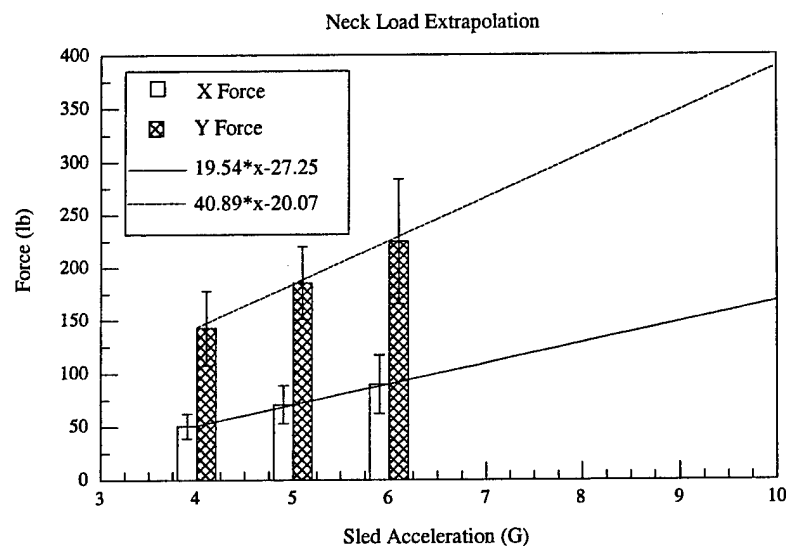


Figure 9. X and Y Neck Load Response Summary and Extrapolation as a Function of Increasing Sled Acceleration

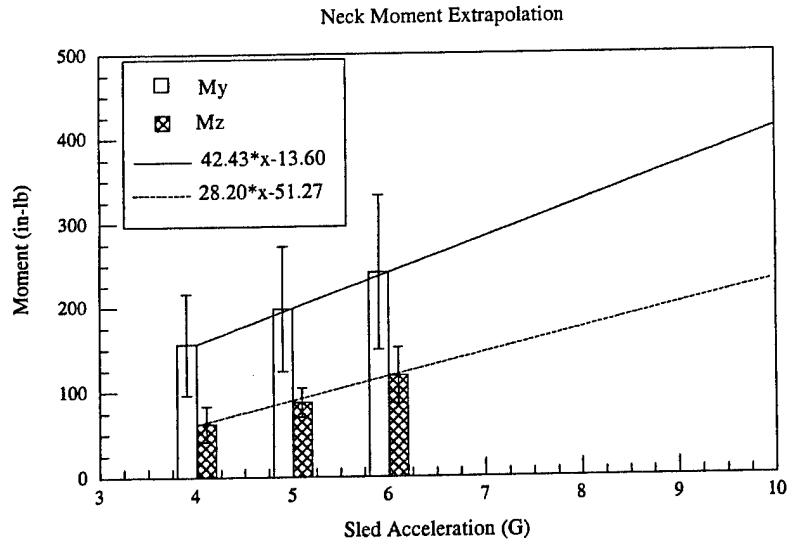


Figure 10. Y and Z Neck Moment Response Summary and Extrapolation as a Function of Increasing Sled Acceleration

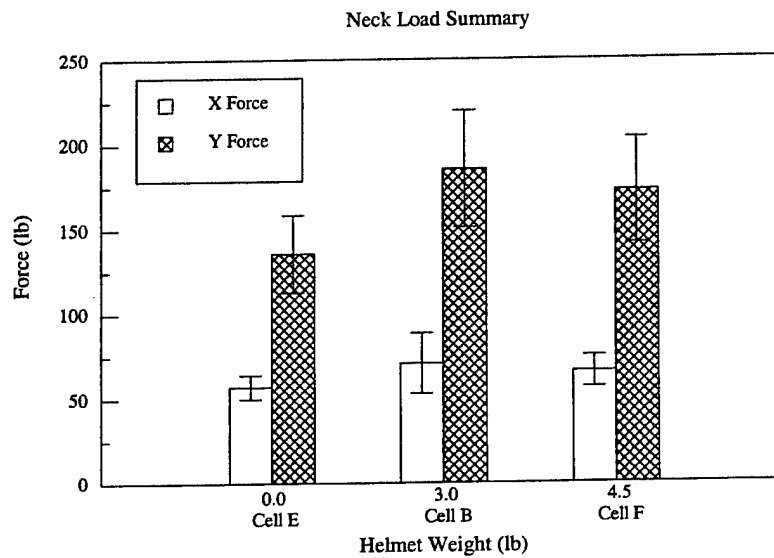


Figure 11. X and Y Neck Load Response Summary as a Function of Helmet Weight

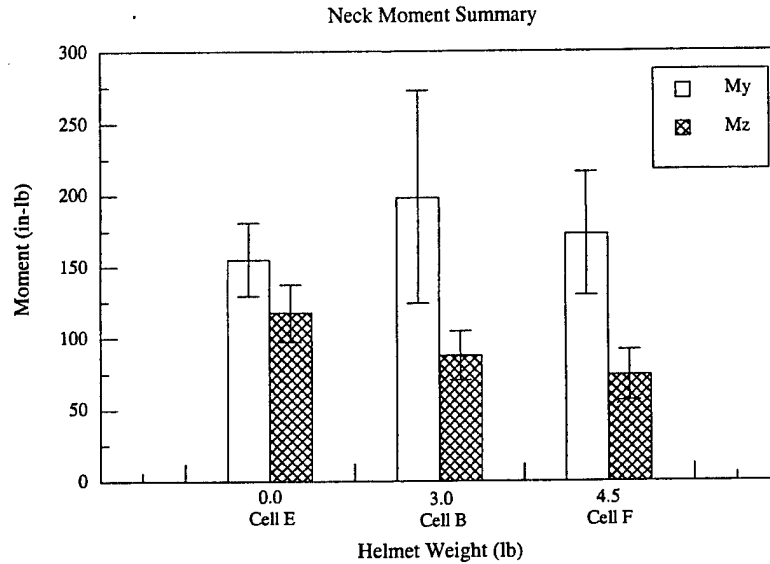


Figure 12. Y and Z Neck Moment Response Summary as a Function of Helmet Weight

The preceding load and moment data were calculated using the program "Neckload3". As described in "Methods" this program does not take into account the external loads on the head resulting from the headrest. Listed below in Table 6 is a summary of the mean peak headrest loads seen in each cell during the acceleration impulses. These headrest forces represent the external loads on the head and remained relatively constant across increasing helmet weight conditions.

Table 6. Summary of Mean Peak Headrest Forces

Cell	Headrest X Force (lbs)	Headrest Y Force (lbs)	Headrest Z Force (lbs)
A	29.28 ± 5.89	61.37 ± 13.14	21.34 ± 7.31
B	35.33 ± 7.84	69.70 ± 10.92	27.36 ± 9.23
C	41.68 ± 12.27	83.50 ± 9.68	27.44 ± 8.19
D	48.07 ± 11.99	36.44 ± 15.14	18.73 ± 6.59
E	37.29 ± 16.92	72.94 ± 8.75	23.17 ± 10.62
F	35.55 ± 7.74	83.26 ± 9.57	23.17 ± 8.07

Gender comparisons were made for the neck loads and moments. Table 7 shows the mean peak Y load and moment values for females and males. Average peak values were plotted against both increasing sled acceleration level and helmet weight, and are shown in Figures 13-16. The female subjects experienced an average of 20.4% lower Z moments and 29.0% greater Y moments than the male subjects (X moment measurements were not taken due to instrumentation

limitations). The Y moment difference was statistically significant within cells B and C, but not within cell F ($\alpha = 0.05$). The Y loads were greater by 20-28% for the female subjects in cells B, C, and F, but were slightly less for females in cells A and E.

Table 7. Gender Comparison of Y Loads and Moments

Y loads (lbs)					Y Moments (in-lbs)				
Cell	Male	Female	% Change	P value	Cell	Male	Female	% Change	P value
A	146.4	136.0	-7.1%	0.456	A	136.4	195.8	43.6%	0.008
B	173.5	221.3	27.5%	0.001	B	176.4	264.5	43.6%	0.004
C	210.0	268.7	28.0%	0.020	C	220.5	302.9	37.4%	0.038
E	138.1	129.4	-6.3%	0.403	E	151.7	164.9	8.7%	0.255
F	163.2	195.6	19.8%	0.017	F	167.5	187.0	11.7%	0.323
Average	166.2	190.2	12.4%	-	Average	170.5	223.0	29.0%	-

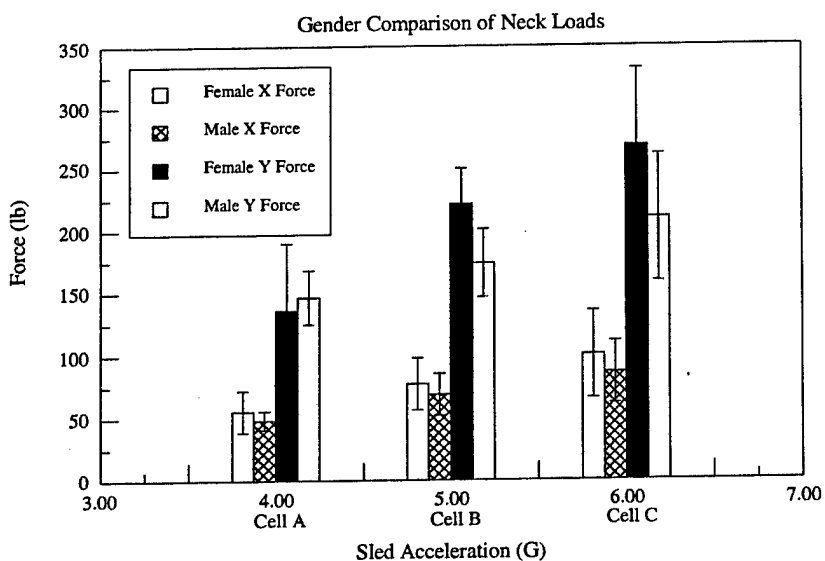


Figure 13. Gender Comparison of X and Y Neck Loads as a Function of Sled Acceleration

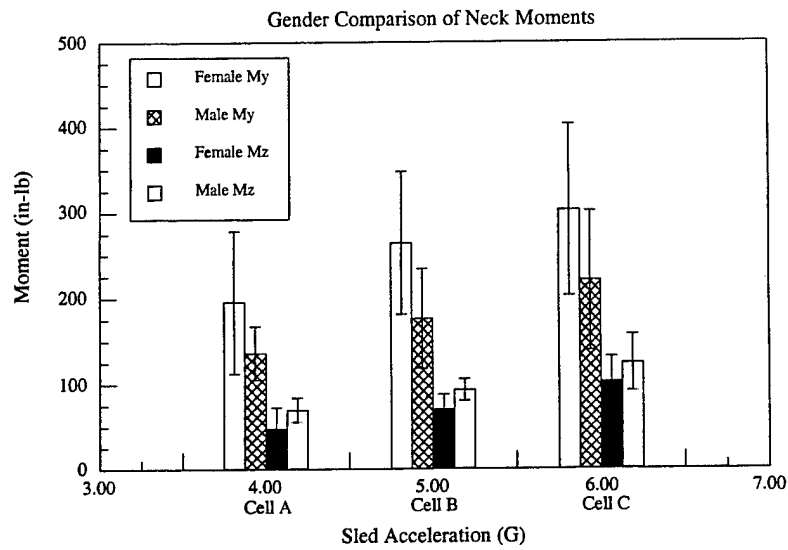


Figure 14. Gender Comparison of Y and Z Neck Moments as a Function of Sled Acceleration

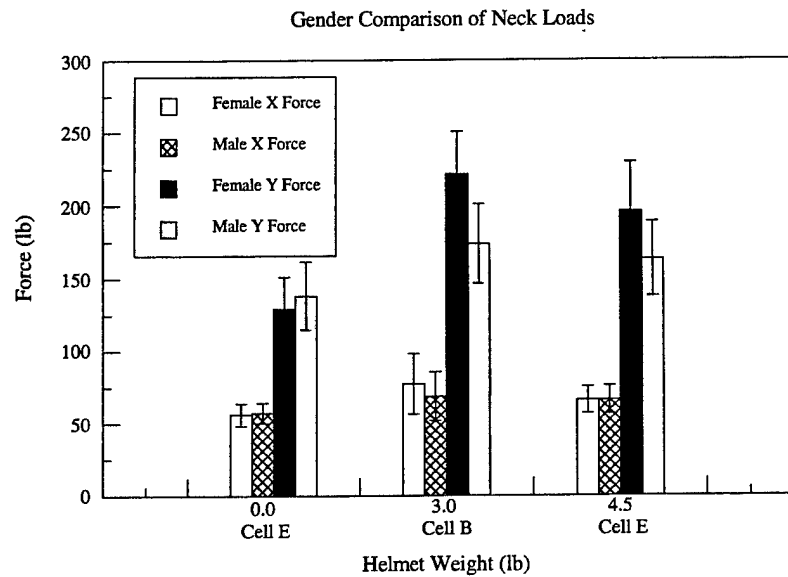


Figure 15. Gender Comparison of X and Y Neck Loads as a Function of Helmet Weight

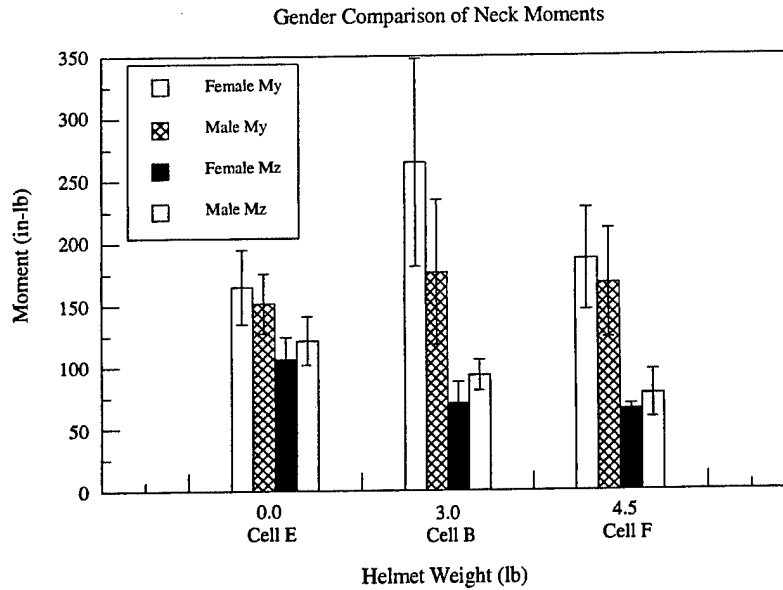


Figure 16. Gender Comparison of Y and Z Neck Moments as a Function of Helmet Weight

A summary of the peak load comparison between contoured (cell E) and flat (cell D) headrests is shown in Figure 17. The Y force generated at the flat headrest decreased by 4.8% compared to the contoured headrest (not statistically different at $\alpha = 0.05$). However, the X force had a significant decrease of 24.7% at the flat headrest ($\alpha = 0.05$). The Z moment was nearly identical across both headrest types, but the Y moment significantly decreased by 15.9% with the flat headrest ($\alpha = 0.05$).

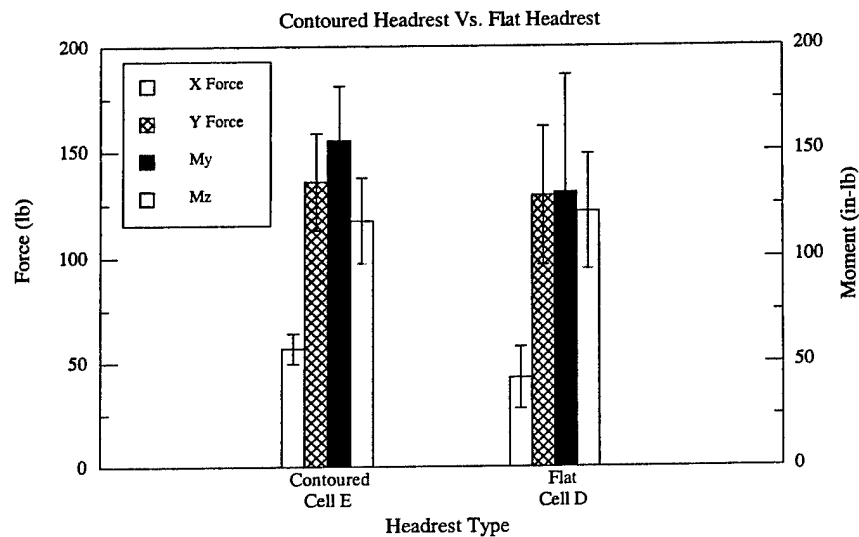


Figure 17. Peak Load Comparison of Contoured Vs. Flat Headrest

Pre-Impact Headrest Loads: The average peak pre-impact headrest loads were examined for differences among the cells to evaluate the effects of subject bracing on the forces seen at the contoured headrest, and are shown in Figures 18 and 19. The headrest pre-impact loads increased with increasing helmet weight, with an 18.2 % increase occurring when the helmet weight was increased from 3.0 lbs (40.1 lbs pre-impact load) to 4.5 lbs (47.4 lbs pre-impact load). This increase however, was not statistically significant at $\alpha = 0.05$. An increase of 12.2% in pre-impact load (not significant at $\alpha = 0.05$) was also observed when the seat acceleration was increased from 5 G (40.2 lbs pre-impact load) to 6 G (45.0 lbs pre-impact load).

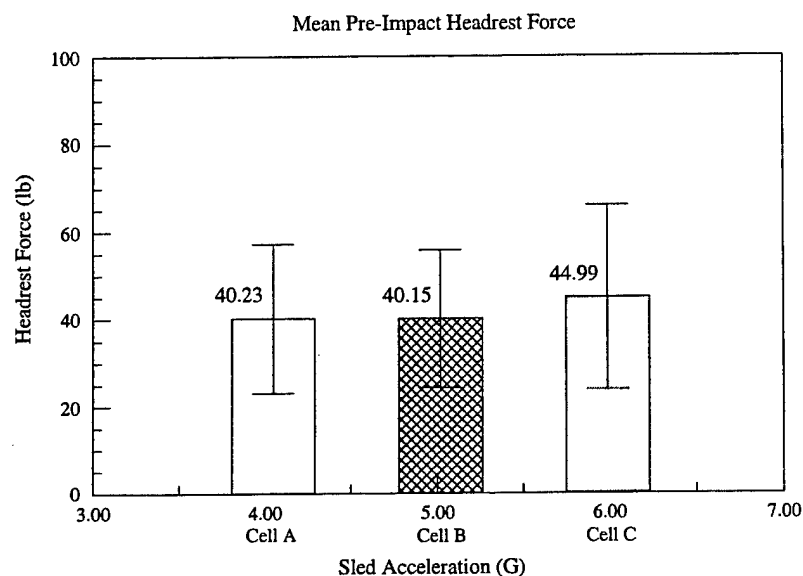


Figure 18. Summary of Pre-Impact Headrest Forces as a Function of Sled Acceleration

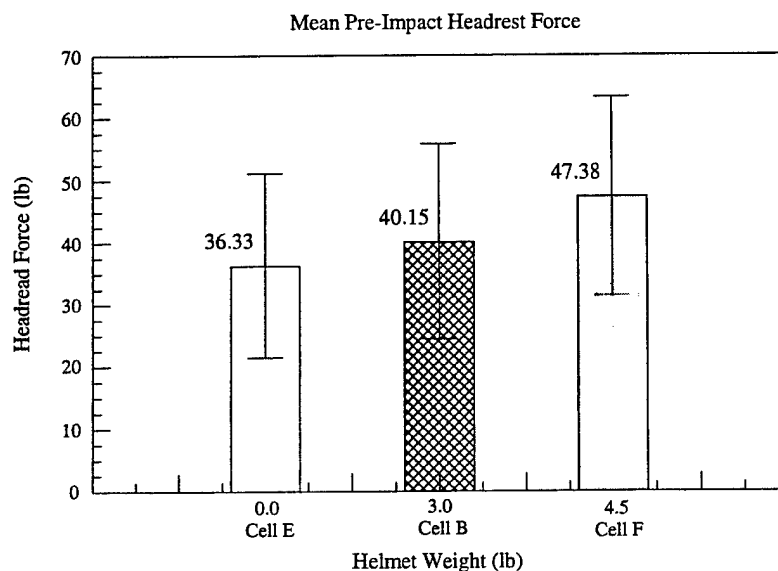


Figure 19. Summary of Pre-Impact Headrest Forces as a Function of Helmet Weight

Gender comparisons were also made for pre-impact headrest forces. These average peak values were plotted against both increasing sled acceleration level and helmet weight, and are shown in Figures 20 and 21. In general, the pre-impact headrest forces remained relatively constant at all acceleration levels, but increased with increasing helmet weight. The female subjects exerted a lesser force against the headrest when compared to the male subjects across all test conditions. The average peak female headrest force was lower by 23.8%, 22.8%, 35.1%, 20.3%, and 26.0% for cells A, B, C, E, and F, respectively, for an average total decrease in female bracing force of 25.6%. This difference was statistically significant at $\alpha = 0.05$ within cells C and F.

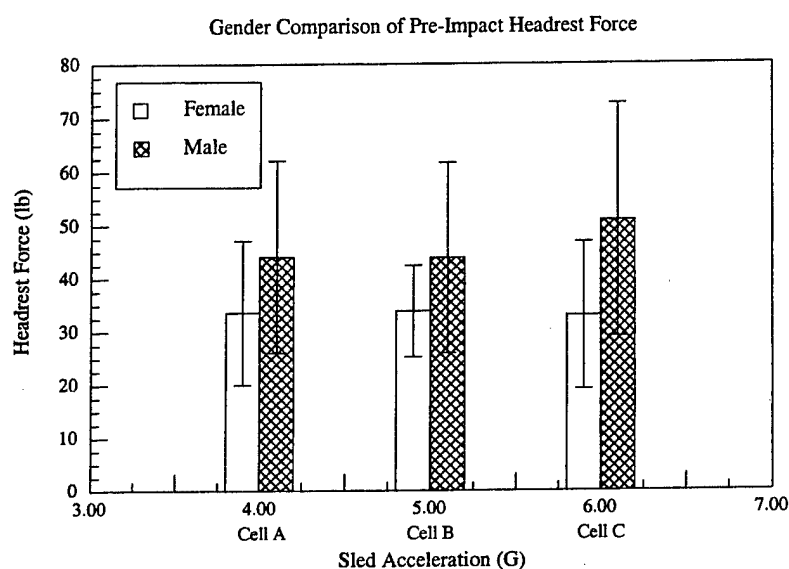


Figure 20. Gender Comparison of Pre-Impact Headrest Forces as a Function of Sled Acceleration

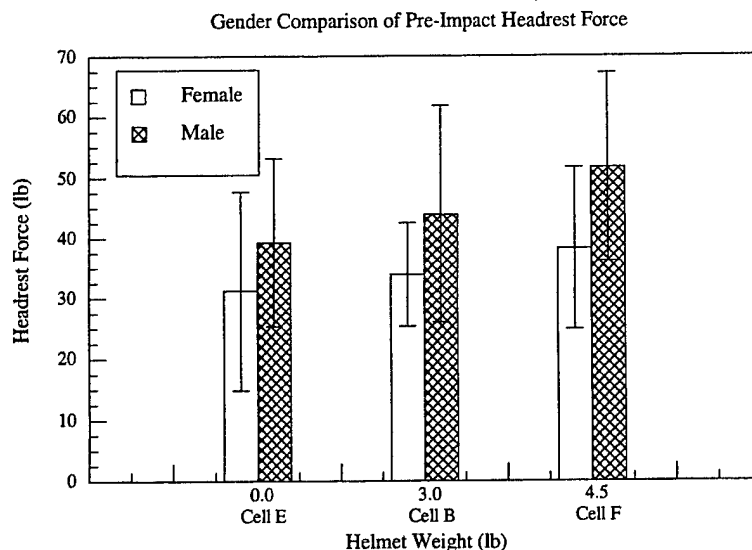


Figure 21. Gender Comparison of Pre-Impact Headrest Forces as a Function of Helmet Weight. The pre-impact loads were also examined for differences between the flat and contoured headrests. An average maximum pre-impact headrest load of 47.4 lbs was observed in cell D (flat headrest). This represents a 30% increase (significant at $\alpha = 0.05$) in pre-impact headrest load as compared to the 36.3 lbs load generated at the contoured headrest (cell E).

Displacement Data: The peak displacement data for the helmet top (or forehead for non-helmeted cells D and E) and mouth for all three axes are listed in Table 8 and were plotted against both increasing sled acceleration and helmet weight, as shown in Figures 22–27. As expected, the largest peak displacement values occurred in the Y direction. Both helmet and mouth displacements increased with increasing sled acceleration levels in the X, Y and Z axes, with the exception of mouth X, which decreased as sled acceleration level was increased from 5 to 6 G. However, mouth X displacement did increase when sled acceleration was increased from 4 to 5 G. As helmet weight was increased from 0 to 3 lbs, all measured displacement values except helmet top X increased. However, as helmet weight was increased from 3 to 4.5 lbs, all measurements in X, Y, and Z axes decreased.

Table 8. Summary of Mean Displacement Data

Test Cell	Helmet Top (Forehead) X (in)	Helmet Top (Forehead) Y (in)	Helmet Top (Forehead) Z (in)	Mouth X (in)	Mouth Y (in)	Mouth Z (in)
A	0.75 ± 0.27	9.18 ± 2.53	2.24 ± 1.21	1.14 ± 1.16	7.98 ± 2.08	1.97 ± 0.89
B	0.98 ± 0.58	10.89 ± 2.17	2.91 ± 0.94	1.82 ± 1.05	9.56 ± 1.57	2.63 ± 1.83
C	1.44 ± 1.16	13.06 ± 1.81	4.01 ± 0.90	1.65 ± 1.18	10.06 ± 1.83	3.55 ± 0.89
D	1.51 ± 0.70	10.55 ± 1.46	1.15 ± 0.66	1.55 ± 1.44	7.69 ± 1.5	1.71 ± 0.74
E	1.28 ± 0.44	8.88 ± 1.27	1.91 ± 0.92	0.83 ± 0.62	8.28 ± 1.18	2.27 ± 0.86
F	0.81 ± 0.31	10.18 ± 1.84	2.3 ± 0.96	1.03 ± 0.87	8.53 ± 1.53	2.47 ± 0.69

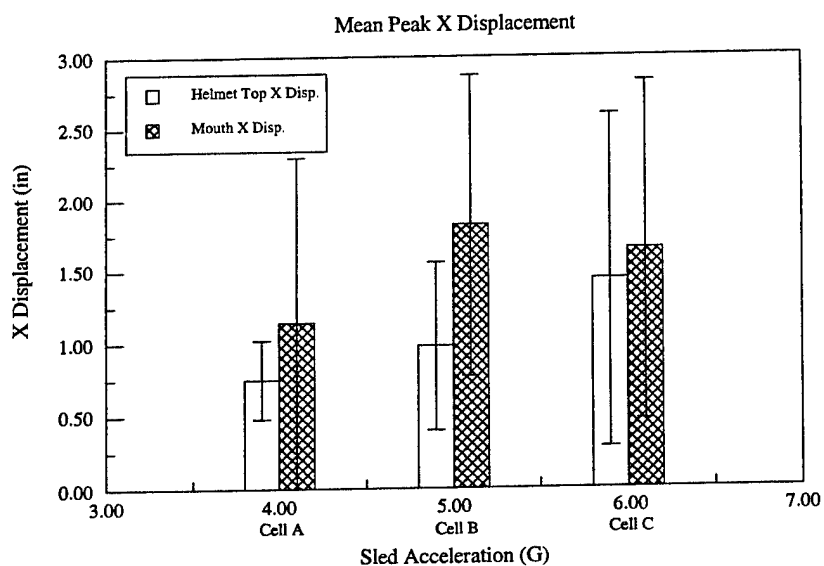


Figure 22. Summary of Peak X Displacement as a Function of Sled Acceleration

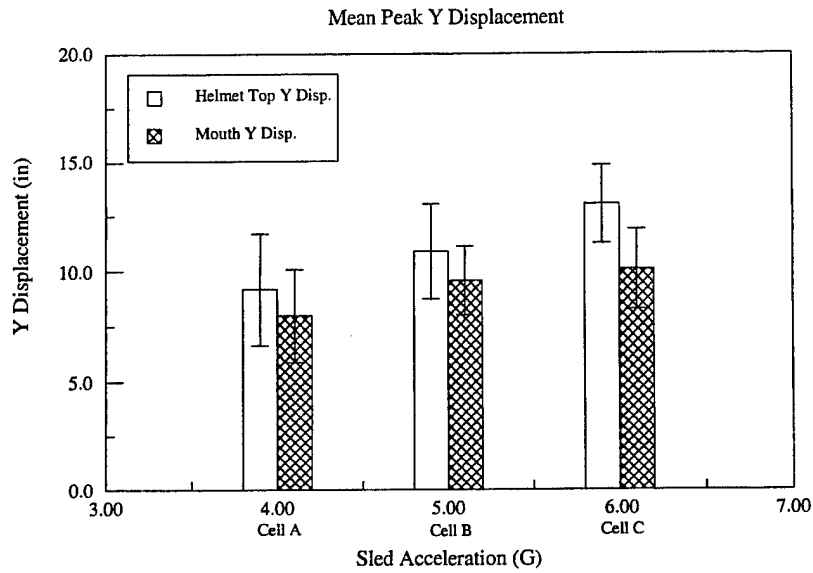


Figure 23. Summary of Peak Y Displacement as a Function of Sled Acceleration

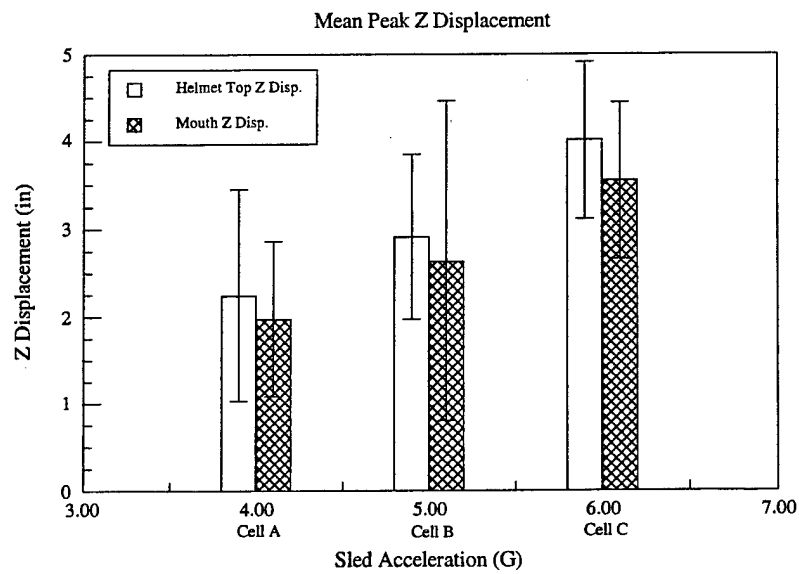


Figure 24. Summary of Peak Z Displacement as a Function of Sled Acceleration

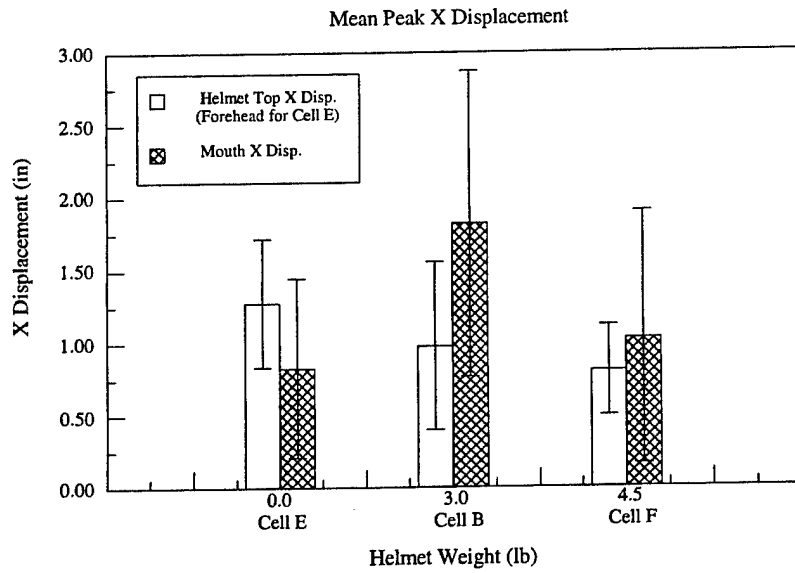


Figure 25. Summary of Peak X Displacement as a Function of Helmet Weight

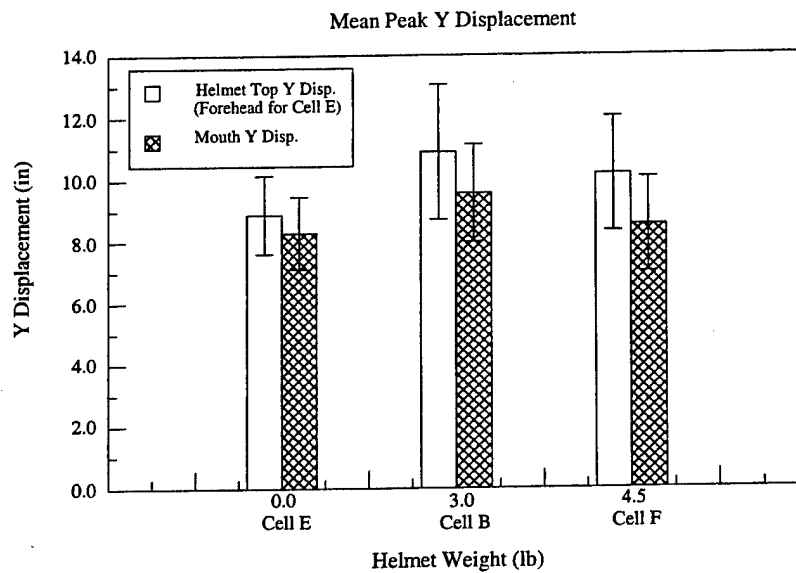


Figure 26. Summary of Peak Y Displacement as a Function of Helmet Weight

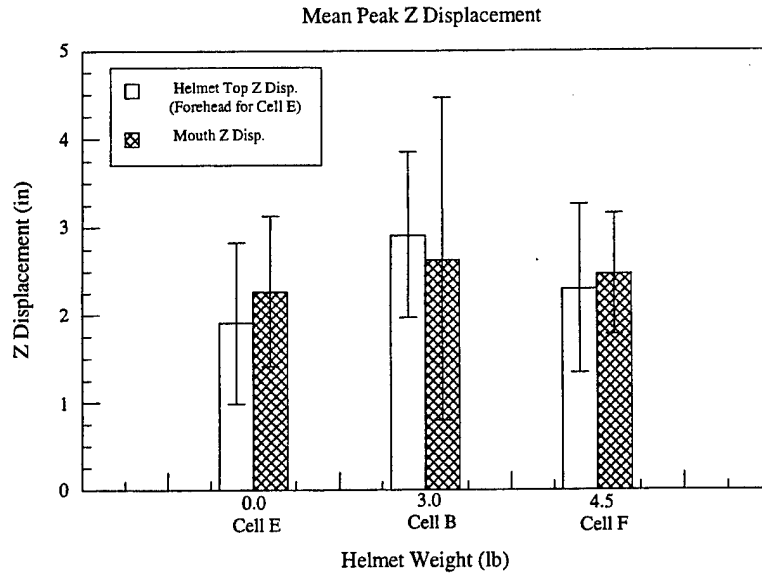


Figure 27. Summary of Peak Z Displacement as a Function of Helmet Weight

Gender comparisons were made for resultant mean displacement data of the helmet top. The resultant displacements were calculated by taking the square root of the sum of squares of the X, Y and Z displacements, done on a point-by-point basis. Table 9 shows that the female displacements were larger for all cells, although none of the differences were statistically significant ($\alpha = 0.05$). These average peak values were plotted against both increasing sled acceleration level and helmet weight, and are shown in Figures 28-29. The female subjects experienced an average of 7.1% greater displacement resultants than the male subjects.

Table 9. Gender Comparison of Resultant Displacements at Helmet Top/Forehead

Mean Peak Resultant Displacement (in)				
Cell	Male	Female	% Change	P Value
A	9.2	10.18	11.1%	0.338
B	11.2	11.9	6.8%	0.475
C	13.5	14.2	5.4%	0.421
E	9.1	9.3	2.3%	0.728
F	10.1	11.1	10.1%	0.261
Average	10.6	11.4	7.1%	-

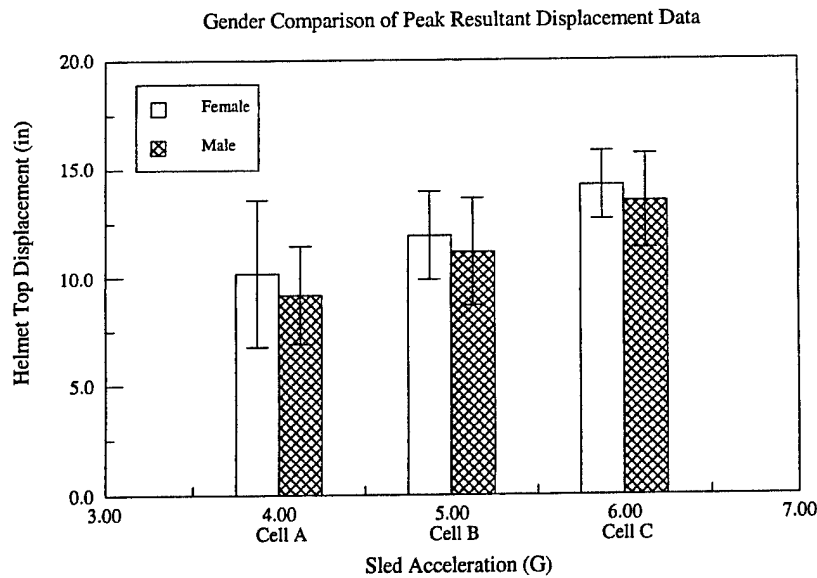


Figure 28. Gender Comparison of Peak Resultant Displacement as a Function of Sled Acceleration

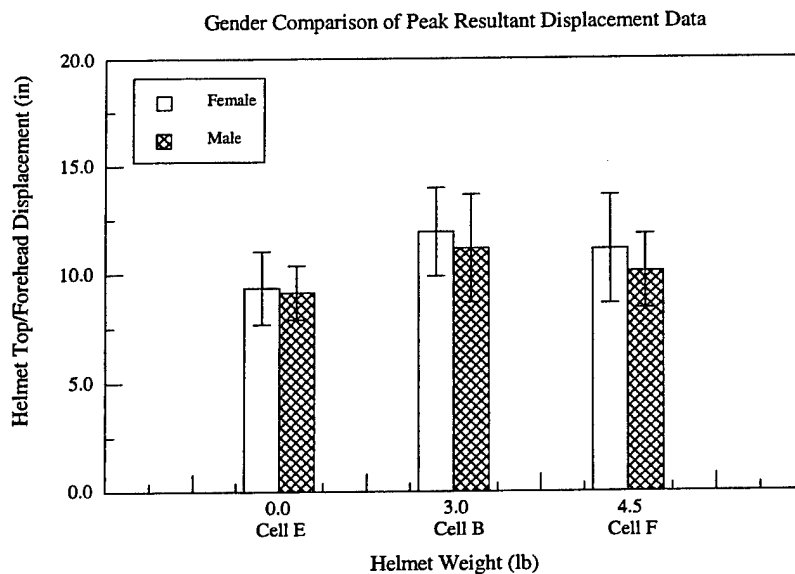


Figure 29. Gender Comparison of Peak Resultant Displacement as a Function of Helmet Weight

A summary of the mean displacement comparison between cell D (flat headrest) and cell E (contoured headrest) is shown in Figure 30. The tests using the contoured headrest had a 7.6% greater (not significant at $\alpha = 0.05$) mouth displacement in the y-axis that was opposite the direction of impact, and a 15.8% smaller (significant at $\alpha = 0.05$) forehead displacement in this axis.

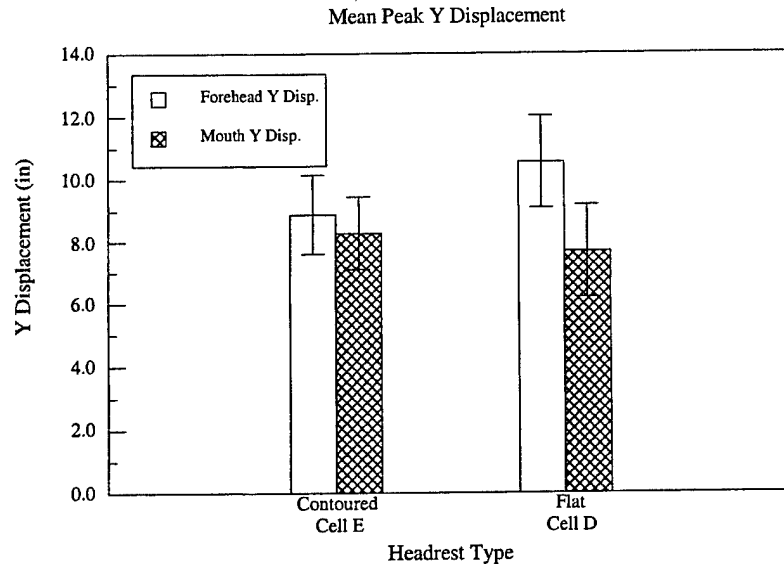


Figure 30. Peak Displacement Comparison of Contoured Vs. Flat Headrest

DISCUSSION

This study demonstrated the effects of input acceleration magnitude and variable helmet weight on displacements, accelerations, and forces experienced by the human body during lateral impact. Figures 4-6 illustrate the increasing accelerations of the body with an increasing acceleration input. The chest and head acceleration peak magnitudes increased linearly with sled acceleration. Both chest and head accelerations peaked after the maximum sled acceleration was reached. The peak input (sled) acceleration was amplified at the head by a factor of approximately 1:1.74 for cells A, B, and C. This general acceleration response is similar to results obtained in previous dynamic response studies by Ewing [2].

The neck loads and moments experienced by our subjects increased linearly with the sled acceleration. The prominent neck load was seen in the direction of sled acceleration (y-axis). The significant Y moments occurred when the subjects' cervical spine went into forward flexion. This peak moment most often took place shortly after the completion of the input acceleration pulse (between 150 and 180 ms). The loads and moments decreased, however, when 1.5 lbs was added to the 3.0 lb helmet. This can be attributed to the subjects' pre-test knowledge of an increase in helmet weight, which encouraged them to brace more forcefully against the headrest before impact. (The non-randomized cell exposure sequence could have also contributed to this effect.) Figure 19 shows that the pre-impact headrest force increased as the helmet weight was increased. Due to the subjects' increased brace, head accelerations were decreased and therefore loads seen at the head-neck joint also decreased. Because the subjects need to tighten their neck muscles in order to brace, it is questionable as to whether the subjects are more likely to strain or injure their neck muscles with or without bracing. More research regarding neck muscle strength and susceptibility to injury is required.

The head displacements also decreased with the added weight, again illustrating the effect of muscle straining on head motion during impact. The headrest forces recorded during impact remained relatively constant across increasing helmet weight conditions (constant sled acceleration). Inertial effects were a significant contributor to the headrest loads in the direction of impact since the headrest with side extension weighed 9.0 lbs.

The test conditions were well tolerated by our subject population, with no incidence of injury. Minor head and/or neck pain was reported in 3% of the tests, which is typical in impact acceleration studies. The maximum calculated Y shear force observed in the male subject population was 382 lbs and the maximum calculated Y moment (flexion or positive My) was 532 in-lbs, both occurring in cell C (6 G, 3.0 lb helmet). The maximum calculated Y shear force and moment for females also occurred in cell C and were 347 lbs and 450 in-lbs, respectively. These were extreme values and not typical in all of the subjects (see Table 5 for averages). Extrapolation of our average dynamic load data indicates that a Y force of 389 lbs and Y moment of 411 in-lbs would be experienced by a subject wearing the 3 lb helmet if tested at a sled acceleration level of 10 G. The extrapolated values would be similar for 4.5 lb helmets assuming the subjects could maintain their bracing techniques at the higher acceleration levels, although this is uncertain. The extrapolated moment for 3 lb helmets would be substantially less than the minimum neck injury threshold of 1680 in-lbs as determined in -Gx tests with cadaveric specimens observed by Mertz and Patrick [4]. Mertz and Patrick also found an injury threshold of 473 lbs shear X force, which is greater than our extrapolated shear Y force value. However, due to the differences in the dynamic response of the cervical spine between the X and Y axes, an accurate comparison of our shear forces with the Mertz and Patrick injury levels could not be made. In addition, since the head X moment was not recorded on the human subjects, conclusions about that measurement also could not be determined.

A comparison of our data to the Naval Biodynamics Laboratory (NBDL) Impact Exposure Guidelines [14] reveals that our subjects were able to tolerate significantly higher neck loads and torques than those listed as safe guidelines in 1989. These guidelines determined by Weiss et al. included Y shear force of 90 lbs and Y moment of 133 in-lbs (both estimated at the occipital condyle (OC), and were based on side impact tests of 7.2 G and 11.3 G with impulse durations of 78 ms and 28 ms, respectively, with no added head-supported weight. We found an average of 225 lbs Y shear force and 240 in-lbs Y moment at a sled acceleration level of 6 G (cell C). Although our variable weighted helmet study was conducted at lower sled acceleration levels, because of the added helmet weight the subjects experienced higher maximum neck loads and torques than in the NBDL study. As previously noted, there were very few reported cases of head or neck pain in our study. However, Weiss et al. reported a common finding of myalgia and headaches, and noted one instance of a stretched brachial plexus. Our results indicate that safe guidelines for sideward impact should be expanded to include the higher neck loads and torques experienced by our subjects during tests with head-supported weight as documented in the results section of this report.

Motion analysis illustrates that the Y, Z, and Resultant head displacements increased linearly with increasing sled acceleration, but decreased with added helmet weight. Again, the decrease observed in head displacements can be attributed to the bracing techniques used by our subjects

when mass was added to the helmets. Upon video observation, the head appears to rotate about the X-axis (roll) until a near maximum deflection angle is reached where the rotation about the Z-axis (yaw) component increases. These observations closely match those made by Ewing [2].

Observing the gender comparisons of the neck loads seen at the OC indicates that the female subjects experienced considerably more forward flexion than the males. Table 7 and Figures 14 and 16 show that a greater Y moment value was seen across all test conditions with the female subjects (29% higher on average). Table 9 and Figures 28-29 support this conclusion by showing that the female head was displaced more than the male head (7.1%) across all test conditions. Females also tended to experience greater lateral neck loads than males in helmet-weighted conditions. As expected with these results, the female subjects exerted significantly lower pre-impact headrest forces than the males (25.6%) across all test conditions.

A comparison between contoured and flat headrests reveals that lower average neck loads were experienced by our subjects when using a flat headrest, while less overall head displacement occurred with the contoured headrest. Subjects braced an average of 30% more forcibly when testing with the flat headrest, which resulted in a statistically significant decrease in the X neck load and Y neck moment (Y neck load decreased slightly) compared to the contoured headrest. As observed in analysis of slow-motion video, the contoured headrest limited linear translation of the head in the lateral direction during impact. Lateral bending motion (rotation about the X-axis, or "roll") was also observed to decrease with the contoured headrest when compared to the flat design. The displacement comparison, seen in Figure 30, illustrates this as the forehead Y displacement increases with the flat headrest. As the head bends laterally, the forehead moves in the direction opposite of impact, and the lower portion of the head continues to rotate about the X-axis of the head. This rotation explains why smaller peak mouth displacements were observed with the flat headrest compared to the contoured headrest. Visual evaluation confirms these data as the subjects experience more lateral bending with the flat headrest. Although the contoured headrest may be beneficial in reducing lateral motion and rotation about the X-axis during lateral accelerations, other factors need to be addressed when designing a headrest. Contoured headrests could potentially apply a concentrated impact to the crewmember's helmet during ejection, thus the aerodynamic forces encountered during ejection need to be considered. Crewmember performance may also be affected by a headrest design if it causes restricted head movement under acceleration or results in reduced side and aft visibility.

CONCLUSIONS

The data from this study provide insight into the mechanisms and thresholds of human neck response during lateral impact, and will be used with data from other human volunteer test programs to develop multi-axial neck injury criteria. The test conditions were well tolerated by the volunteer subjects with no incidence of injury. The forces and moments generated at the head/neck joint during the tests were well within known injury limits set by previous cadaver studies, and were extrapolated out to higher acceleration levels to establish maximum safe levels of human neck tolerance. Because the average maximum neck load and torque values experienced by our subjects were higher than previous safe guideline values published by the

Naval Biodynamics Laboratory, it is proposed that new guidelines be developed to encompass helmets of various inertial properties.

These tests also demonstrated how a subject's trained response and bracing technique produced a more constant load at the OC across variable helmet weights. At the levels tested, bracing can decrease the loads seen at the head-neck joint, although the potential for neck muscle strain or injury due to excessive bracing has not yet been investigated. In general, the male subjects were more successful at bracing to decrease the moments inflicted on the head-neck joint. The female subjects may therefore be more susceptible to a neck injury during lateral impacts due to higher observed Y moments (flexion) during such an impact. Overall, the subjects were inclined to brace more forcibly when weight was added to the helmet and when bracing against a flat headrest. The results also demonstrated that contoured headrests are useful in restricting rotation about the X-axis (or roll) during side impacts. The contoured headrest offers improved stability and enables the subject to better brace during high accelerations. Other factors, however, such as the aerodynamic effects on the head resulting from a contoured headrest, potential for concentrated impact areas on the headrest, and the effect of the headrest shape and size on pilot performance also need to be taken into account when designing an ejection seat headrest.

REFERENCES

1. Buhrman, J.R., C.E. Perry, and F.S. Knox III (1994). Human and Manikin Head/Neck Response to +Gz Acceleration When Encumbered by Helmets of Various Weights. *Aviation, Space, and Environmental Medicine*, 65, 1086-1090.
2. Ewing, C.L. et al (1978). Dynamic Response of Human and Primate Head and Neck to +Gy Impact Acceleration. HS-803-058, *Naval Aerospace Medical Research Lab Detachment*, New Orleans, LA.
3. Eppinger, R., E. Sun, S. Kuppa (2000). Supplement: Development of Improved Injury Criteria for the Assessment of Advanced Automotive Restraint Systems – II.
4. Mertz H.J., L.M. Patrick (1971). Strength and response of the human neck. *Proceedings of the Fifteenth Stapp Car Crash Conference, Society of Automotive Engineers*, Warrendale, PA: SAE
5. Perry, C.E. (1998). Effects of Variable Helmet Weight on Human Response to +Gy Impact. AFRL/HESA Protocol 98-03, Wright Research Site Institutional Review Board, Wright-Patterson AFB OH.
6. Perry, C.E. (1998). The Effect of Helmet Inertial Properties on Male and Female Head Response During +Gz Impact Accelerations. *SAFE Journal*, 28(1), 32-38.
7. Perry, C.E. and J.R. Buhrman (1997). Head Mounted Display (HMD) Head and Neck Biomechanics. In J.E. Melzer and K. Moffitt (Eds.), *Head Mounted Displays: Designing for the User (Chap.6, pp 147-174)*. New York: McGraw-Hill.
8. Perry, C.E. and J.R. Buhrman (1996). Effect of Helmet Inertial Properties of the Biodynamics of the Head and Neck During +Gz Impact Accelerations. *SAFE Journal*, 26(2), 34-41.
9. Perry, C.E. and J.R. Buhrman (1995). Effect of Helmet Inertial Properties on Head and Neck Response During +Gz Impact Accelerations. *Proceedings of the 16th Annual International Gravitational Physiology Meeting*, March 1995.
10. Perry, C.E., J.R. Buhrman, and F.S. Knox III (1993). Biodynamic Testing of Helmet Mounted Systems. *Proceedings of the 37th Annual Human Factors and Ergonomics Society Meeting*, 1, 79-83.
11. Perry, C.E., A.R. Rizer, J.S. Smith, and B. Anderson (1997). Biodynamic Modeling of Human Neck Response During Vertical Impact. *SAFE Journal*, 27(3), 183-191.
12. Strzelecki J.P. (1994). Loads Induced in the Lumbar Spine of Seated Restrained Humans by Sideward (+Gy) Impact. *AsMA Conference*, San Antonio, TX.

13. Taylor, J.K. (1990). Statistical Techniques For Data Analysis. Boca, Raton, FL: CRC Press, Inc. (through Lewis Publishers, Inc.)
14. Weiss, M.S., D.L. Matson, S.V. Mawn (1989). Guidelines for Safe Human Exposure to Impact Acceleration – Update A. NBDL-89R003, *Naval Biodynamics Laboratory*, New Orleans, LA.

APPENDIX A

Test Configuration and Data Acquisition System

TEST CONFIGURATION AND
DATA ACQUISITION SYSTEM FOR THE
EFFECTS OF VARIABLE WEIGHT ON HUMAN
RESPONSE TO VARIED +G_y IMPACT

(VWHGY Study)

Prepared under
Contract F3301-96-DJ001

May 2000

DynCorp
Human Effectiveness Division
Building 824, Area B
Wright-Patterson AFB, Ohio 45433

Table of Contents

1	TEST FACILITIES	34
1.1	HORIZONTAL IMPULSE ACCELERATOR	34
2	TEST EQUIPMENT	35
3	TEST SUBJECTS	37
4	TEST CONDITIONS MATRIX.....	38
5	INSTRUMENTATION	38
5.1	ACCELEROMETERS	39
5.2	LOAD CELL TRANSDUCERS	39
5.3	SEAT COORDINATE REFERENCE SYSTEM.....	42
5.4	TRANSDUCER CALIBRATION	45
6	DATA ACQUISITION	45
6.1	EME DAS-64 DATA ACQUISITION AND STORAGE SYSTEM	45
6.2	SELSPOT MOTION ANALYSIS.....	46
6.3	KODAK HIGH SPEED VIDEO	48
7	DATA PROCESSING	48

Table of Figures

Figure A-1: Horizontal Impulse Accelerator (HIA)	35
Figure A-2: VWHGY Test Setup	35
Figure A-3: Modified HGU-55/P Helmet	36
Figure A-4: Load Link Configuration	40
Figure A-5: Coordinate Reference and Sensor Locations.....	42
Figure A-6: Seat Adjustment Details.....	44
Figure A-7: SELSPOT Position Reference Structure	47
Figure A-8: Selspot Target Locations	47

Table of Tables

Table A-1: Test Equipment Summary	37
Table A-2 VWHGY Variable Conditions	38
Table A-3: Sensor Setup and Calibration Log.....	50

INTRODUCTION

DynCorp, Human Effectiveness Division prepared this report for the Air Force Research Laboratory, Human Effectiveness Directorate, Biodynamics and Acceleration Branch under Air Force contract F3301-96-DJ001. It describes the test facility, test configurations, data acquisition and analysis, and the instrumentation procedures used for the Effects of Variable Helmet Weight on Human Response To +G_y Impact (VWHGY Study). Two hundred six tests were conducted between 3 Aug 1998 and 18 Feb 1999 on the HIA.

Test Facilities

1.1 Horizontal Impulse Accelerator

The Horizontal Impulse Accelerator (HIA) system consists of a 24-inch HYGE actuator, a 4-foot x 8-foot test sled, and a 240-foot track. The HYGE actuator is a hydraulic/pneumatic system manufactured by the Bendix Corporation. Figure A-1 is a cross-sectional view of the actuator system. It has front and rear cylinder sections each with a hydraulically controlled floating piston for controlling the volumes in the gas pressure chambers. The energy of high-pressure gas in the load chamber propels the thrust piston to create the acceleration pulse for the test sled. The system is armed by pressurizing the set chamber with nitrogen to seal the thrust piston to the orifice plate. Then, the load chamber is pumped up with compressed air approximately six times the set pressure depending on test conditions. Trigger pressure breaks the orifice seal and exposes the full surface area of the thrust piston to the load pressure for test initiation. The geometric profile of the metering pin attached to the face of the thrust piston varies the orifice area and controls the shape of the acceleration pulse. Various acceleration profiles (half-sine, trapezoidal, etc.) are available by changing the metering pin. The system can accelerate a test payload of 2000 pounds up to 115 Gs with a duration of 0.175 seconds. With this system, test conditions are repeatable to $\pm 2\%$. The 2000-pound test sled glides along the track rails on 12 Delrin pads with a Delrin reaction guide at each corner to minimize off-axis accelerations. It can carry up to a 2500 pound test payload. It is equipped with gas-operated brakes, which are applied as needed to stop the sled prior to the end of the track. The track rails are made of 1-inch thick mild steel. A complete description of the HIA system is given in AMRL TR 76-8.

The HIA system simulates impact phenomena by accelerating a test payload from rest. The test subject experiences dynamic loads equivalent to the forces experienced during an actual impact. There are several laboratory control advantages in having the initial position at rest, which include: accurate positioning of the subject prior to the test; no extraneous forces present prior to the test; precise control of test initiation and data collection systems; and rapid, repeatable reset of test conditions.

BEST AVAILABLE COPY

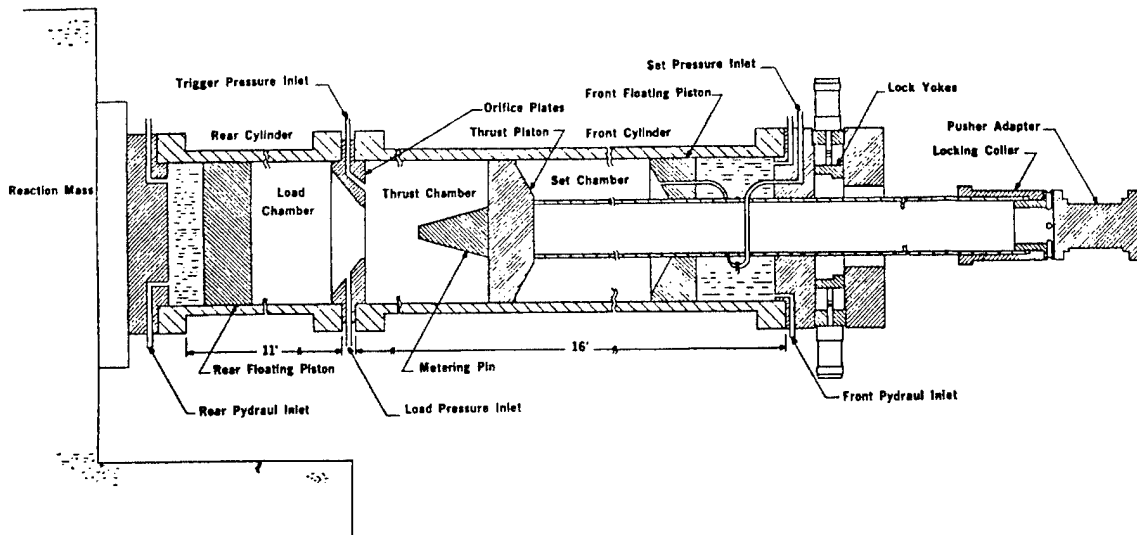


Figure A-1. Horizontal Impulse Accelerator (HIA)

Test Equipment

The 40-G test seat fixture was used for all the tests. It was mounted to the sled deck in the +G_y orientation. Figure A-2 shows the complete setup.



Figure A-2. VWHGY Test Setup

BEST AVAILABLE COPY

The subjects were restrained in the seat by two shoulder straps and a lap belt. No cushions were used; the subjects sat on the bare seat. The seat was equipped with adjustable supports for the hips, knees, and feet. The adjustment provided for accommodation of a wide range of subjects. The adjustment mechanisms are shown in the Details of Figure A-6. The subjects' hands and feet were restrained by Velcro loops. For the hands, the loops were secured to the subjects thighs, and for the feet, they went around the footrest.

A modified HGU-55/P helmet was used. It had brackets over both earcups so weight could be added symmetrically to the helmet as required. Figure A-3 shows the details of the weight mounting.

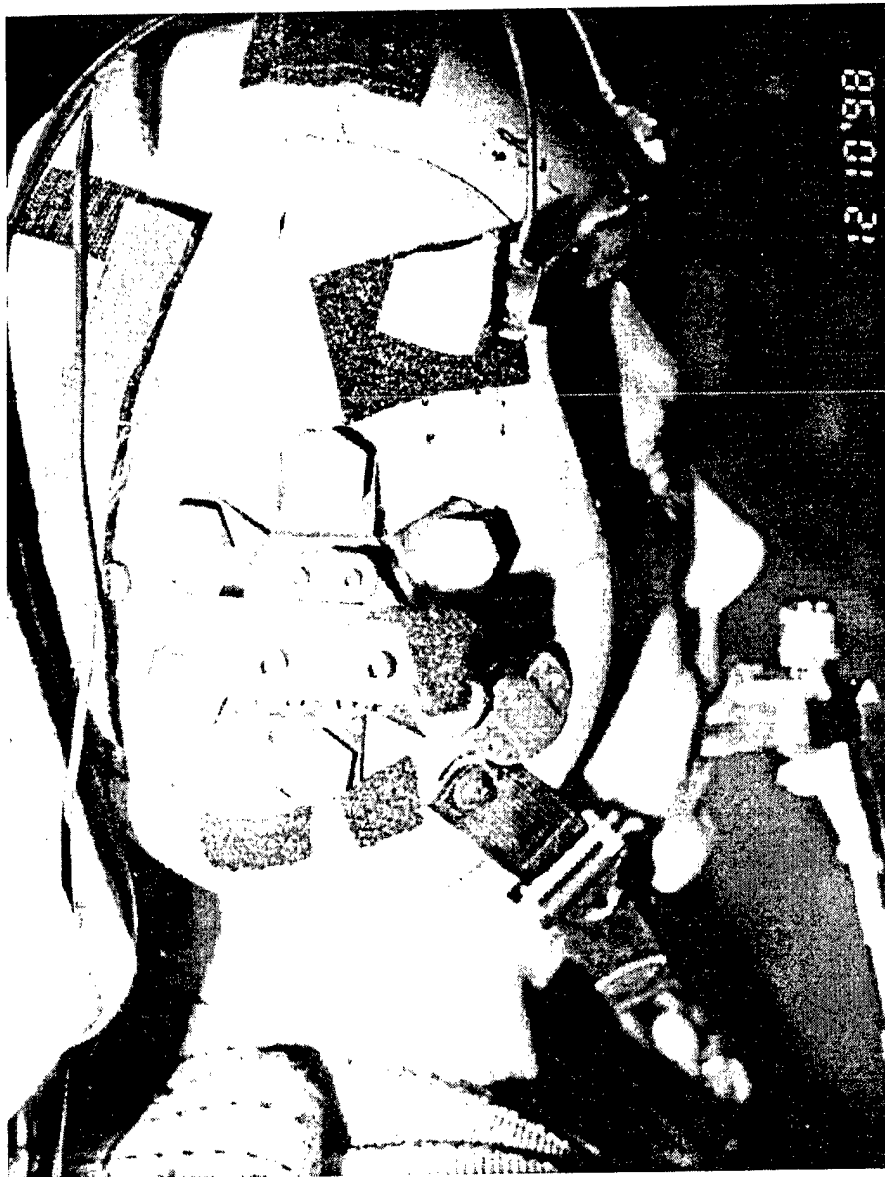


Figure A-3. Modified HGU-55/P Helmet

Table A-1 summarizes the facilities and equipment used for this study.

Equipment	ID
Facility	HIA
Pin Number	11
Seat Fixture	40 G
Seat Cushion	None
Harness	PCU-15/P
Helmet	Modified HGU-55/P
Inertial Reel	None
Lap Belt	MA5
Oxygen Mask	None
NVG/HMD	None
Neg-G Strap	None
Head Rest Position	In Line
Lap Belt Adjuster	
Seat Pan/Seat Back Position	90° / Reclined 13°

Table A-1. Test Equipment Summary

Test Subjects

Human volunteers and manikins were used for this study. The data on humans was the focus of the study. Manikin subjects were used only to investigate the loads experienced in the various profiles prior to testing with the volunteers. An instrumented ADAM manikin was used for the safety trials prior to running volunteers. The human subjects wore cutoff long underwear, socks, and the modified HGU-55/P helmet.

Along with the subject, the sled was ballasted to maintain a constant weight and a consistent impact pulse. The ballast was set to two hundred twenty pounds minus the weight of the subject.

Test Conditions Matrix

Cell ID	G Level (G)	Variable Weight Helmet (lbs)	Headrest
A	4	3	Contoured
B	5	3	Contoured
C	6	3	Contoured
D	5	0	Flat
E	5	0	Contoured
F	5	4.5	Contoured

Table A-2. VWHGY Variable Conditions

Variable weight helmet is for the specially modified HGU-55/P flight helmet plus any added weight. The zero weight condition is for no helmet.

Instrumentation

Accelerometers and load transducers were chosen to provide the optimum resolution over the expected test load range. Full-scale data ranges were chosen to provide the expected full-scale range plus 50% to assure the capture of peak signals. All transducer bridges were balanced for optimum output prior to the start of the program. The accelerometers were adjusted for the effect of gravity using computer processing software. The component of a one G vector in line with the force of gravity that lies along the accelerometer axis was added to each accelerometer.

The test coordinate systems, used by the AFRL/HEPA laboratory, are right-handed with the Z-axis parallel to the seat back and positive upward. The X-axis is perpendicular to the Z-axis and positive eyes forward from the subject. The Y-axis is perpendicular to the X and Z-axes according to the right hand rule. The origin of the seat coordinate system is designated as the seat reference point (SRP). The SRP is at the midpoint of the line segment formed by the intersection of the seat pan and seat back. All vector components (for accelerations, forces, moments, etc.) were positive when the vector component (X, Y and Z) was in the direction of the positive axis.

The laboratory uses three primary coordinate systems. One is referenced to the device carriage (termed sled coordinates for the HIA, and carriage coordinates for the VDT). The sled coordinates have +X fixed in the down track direction. Positive Z is up, and +Y is to the left. The carriage coordinates on the VDT fix +Z upward along the rails, with +X along eyes forward, and +Y to the left. The other is the seat coordinate system described in the previous paragraph. These systems will differ by any angular orientation of the

seat versus the device carriage. Data values labeled sled or carriage are referenced to the respective device carriage. The third coordinate system is for sensors located on the subject. It is referred to as the subject or manikin coordinate system. It also uses the right-handed convention. Positive X is along eyes forward, positive Z is up through the top of the head, and Y is positive through the left ear. In almost all cases, the subject coordinate system is aligned with the seat system initially, but the subject references move with the subject during an impact reaction. Data values labeled head or chest, for instance, are referenced to the subject coordinate system. A diagram of the seat coordinate system with a seat sketch and sensor locations is shown in Figure A-5.

The linear accelerometers were wired to provide a positive output voltage when the acceleration experienced by the accelerometer was applied in the +X, +Y and +Z directions. The load cells were wired to provide a positive output voltage when the force exerted by the load cell on the subject was applied in the +X, +Y or +Z direction.

The sled linear accelerometers were wired to provide a positive output voltage when the acceleration experienced by the accelerometer is applied in the +X, +Y or +Z directions. The sled velocity tachometer was wired to provide a positive output voltage when the sled moves in the +X direction.

The carriage velocity and sled velocity were measured using Globe Industries tachometers Model 22A672-2. The rotor of the tachometer was attached to an aluminum wheel with a rubber "O" ring around its circumference to assure good rail contact. The wheel contacted the track rail and rotated as the carriage (or sled) moved, producing an output voltage proportional to the velocity.

1.2 Accelerometers

The specific accelerometers used in this study are listed in the Instrumentation Tables at the end of this report. The tables also provide channel assignments and sensor sensitivities.

Head accelerations were measured by a package of three linear (for X, Y, and Z) and two angular (for R_Y and R_Z) accelerometers mounted on a Lucite bite block held by the subjects. The chest accelerations were measured by an external package of linear and angular accelerometers mounted to the subjects harness. The location of the seat accelerometers is shown in Figure A-5.

1.3 Load Cell Transducers

The specific load cells used are listed in the Instrumentation Tables at the end of this report. The tables also provide channel assignments and sensor sensitivities. The locations of the various load cells are shown in Figure A-5.

Shoulder/anchor forces were measured using three AAMRL/DYN 3D-SW and one Michigan Scientific 4000 tri-axial load cells, each capable of measuring forces in the X, Y and Z directions. The lap anchor force tri-axial load cells were located on separate brackets mounted on the side of the seat frame parallel to the seat pan. The shoulder strap force tri-axial load cell was mounted on the seat frame between the seat back support plate and the headrest.

Left, right and center seat pan forces were measured using three load cells and three load links. The three load cells included two Strainsert Model FL2.5U-2SGKT and one FL2.5U-2SPKT load cells. DynCorp fabricated the three load links, Figure A-4, with Micro Measurement Model EA-06-062TJ-350 strain gages.

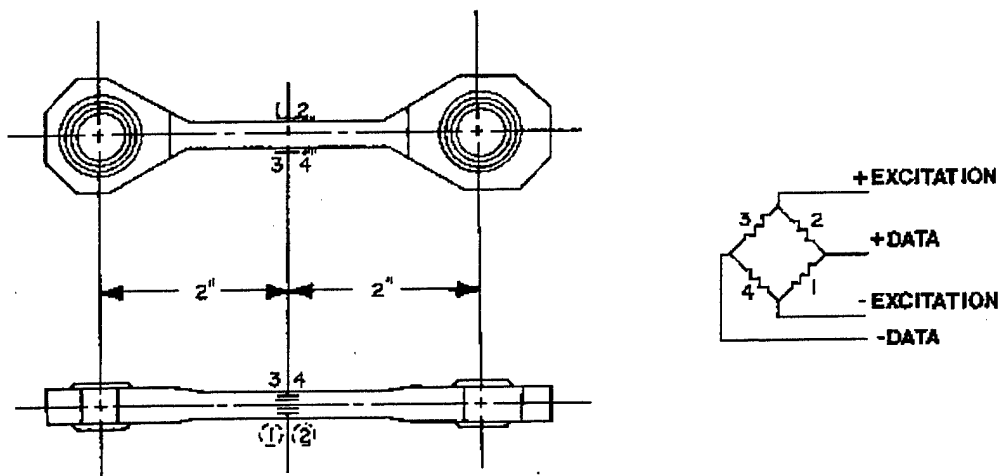


Figure A-4. Load Link Configuration

All six measurement devices were located under the seat pan support plate. The load links were used for measuring loads in the X (two links) and Y (one link) directions. Each load link housed a swivel ball, which acted as a coupler between the seat pan and load cell mounting plate. The Strainsert load cells were used for measuring loads in the z direction.

Left, right and center seat back forces were measured using three Strainsert Model FL2.5U-2SPKT load cells. Top, bottom and center seat back link forces were measured using three load links, which are identical to the links described for the seat pan. All six measurement devices were located behind the seat back support plate. The load links were used for measuring loads in the Y (two links) and Z (one link) directions. The Strainsert load cells were used for measuring loads in the x direction.

Headrest X, Y and Z forces were measured using one AAMRL/DYN 3D-SW triaxial load cell. The load cell was mounted on a rectangular mounting plate, which was attached to the upper seat back. The headrest was attached directly to the load cell, and could be adjusted up or down depending on the location of the subject's head.

The Hip and Knee supports were used for subject safety, but they were not instrumented for this study. Nor was the footrest. No forces were measured at these locations.

1.4 Seat Coordinate Reference System

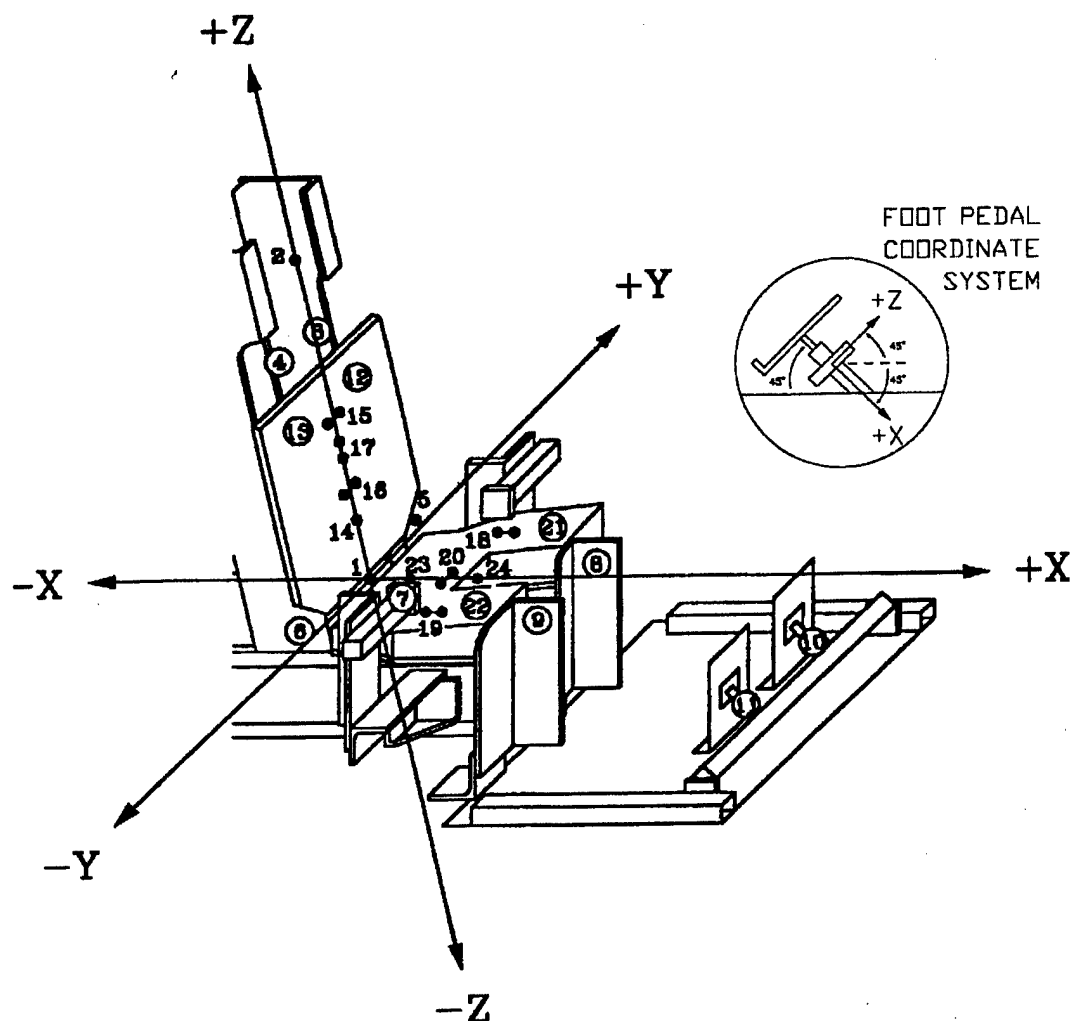


Figure A-5. Coordinate Reference and Sensor Locations

NO.	DESCRIPTION	NO.	DESCRIPTION
1	SEAT REFERENCE POINT	13	RIGHT SEAT BACK X FORCE
2	HEAD FORCE	14	CENTER SEAT BACK X FORCE
3	LEFT SHOULDER BELT FORCE	15	TOP SEAT BACK LINR Y FORCE
4	RIGHT SHOULDER BELT FORCE	16	BOTTOM SEAT BACK LINK Y FORCE
5	LEFT LAP BELT FORCE	17	CENTER SEAT BACK LINR Z FORCE
6	RIGHT LAP BELT FORCE	18	LEFT SEAT PAN LINR X FORCE
7	RIGHT HIP Y FORCE (not used)	19	RIGHT SEAT PAN LINR X FORCE
8	LEFT KNEE Y FORCE (not used)	20	CENTER SEAT PAN LINR Y FORCE
9	RIGHT KNEE Y FORCE (not used)	21	LEFT SEAT PAN Z FORCE
10	LEFT FOOT FORCE (not used)	22	RIGHT SEAT PAN Z FORCE
11	RIGHT FOOT FORCE (not used)	23	CENTER SEAT PAN Z FORCE
12	LEFT SEAT BACK X FORCE	24	SEAT X AND Y ACCELEROMETER

ALL DIMENSIONS ARE REFERENCED TO THE SEAT REFERENCE POINT (SRP). THE SEAT REFERENCE POINT IS LOCATED AT THE INTERSECTION OF THE SEAT PAN CENTER LINE AND THE SEAT BACK CENTER LINE (Z AXIS).

CONTACT POINT DIMENSIONS IN INCHES (CM)

NO.	X		Y		Z	
1	0.00	(0.00)	0.00	(0.00)	0.00	(0.00)
2	-6.85	(-17.39)	-0.54	(-1.37)	33.08	(84.03)
3	-3.18	(-8.07)	2.02	(5.14)	26.02	(66.10)
4	-3.18	(-8.07)	-2.87	(-7.28)	26.07	(66.21)
5	2.21	(5.61)	8.88	(22.56)	-2.00	(-5.08)
6	2.01	(5.11)	-9.14	(-23.21)	-2.11	(-5.37)
7	9.63	(24.45)	-8.68	(-22.05)	4.23	(10.75)
8	20.71	(52.60)	2.69	(6.82)	5.07	(12.89)
9	20.81	(52.85)	-8.41	(-21.35)	5.12	(13.01)
10	44.22	(112.31)	5.98	(15.18)	-7.50	(-19.06)
11	44.09	(112.00)	-5.94	(-15.10)	-7.52	(-19.11)
10	43.02	(109.28)	5.96	(15.15)	-6.67	(-16.93)
11	43.02	(109.28)	-6.08	(-15.45)	-6.73	(-17.09)
12	-1.51	(-3.83)	5.46	(13.87)	17.50	(44.46)
13	-1.51	(-3.83)	-6.28	(-15.95)	17.33	(44.01)
14	-1.51	(-3.83)	-1.98	(-5.02)	5.24	(13.31)
15	-2.10	(-5.33)	-2.36	(-6.00)	17.44	(44.31)
16	-2.10	(-5.33)	3.28	(8.32)	9.42	(23.92)
17	-2.10	(-5.33)	-0.34	(-0.87)	14.62	(37.14)
18	13.54	(34.39)	6.19	(15.71)	-3.14	(-7.98)
19	13.42	(34.09)	-5.90	(-14.99)	-3.14	(-7.98)
20	8.74	(22.19)	2.03	(5.15)	-3.14	(-7.98)
21	17.55	(44.58)	5.04	(12.80)	-2.40	(-6.10)
22	17.60	(44.71)	-5.02	(-12.74)	-2.40	(-6.10)
23	6.30	(15.99)	0.17	(0.42)	-2.40	(-6.10)
24	13.64	(34.65)	0.17	(0.42)	-4.70	(-11.95)

THE SEAT ACCELEROMETER MEASUREMENTS (ITEM 24) WERE TAKEN AT THE CENTER OF THE ACCELEROMETER BLOCK. THE CONTACT POINT IS THE POINT ON THE LOAD CELL AT WHICH THE EXTERNAL FORCE IS APPLIED. THE ANCHOR HARNESS ATTACH POINT WAS USED FOR LOAD CELLS 3, 4, 5 & 6. THE MEASUREMENTS FOR THE RIGHT HIP LOAD CELL (ITEM 7) WERE TAKEN WITH THE VERTICAL ADJUSTMENT BRACKET (A) LOCATION 2 AND THE HORIZONTAL ADJUSTMENT BRACKET (B) LOCATION 0, Figure A-6. (not used) THE MEASUREMENTS FOR THE RIGHT KNEE LOAD CELL (ITEM 9) WERE TAKEN WITH THE VERTICAL ADJUSTMENT BRACKET (C) POSITION 2 AND THE HORIZONTAL ADJUSTMENT BRACKET (D) POSITION 1, Figure A-6. (not used) THE MEASUREMENTS FOR THE FOOT LOAD CELLS (ITEMS 10 & 11) WERE TAKEN WITH THE ADJUSTMENT BRACKET (E) LOCATION 1, Figure A-6. (not used)

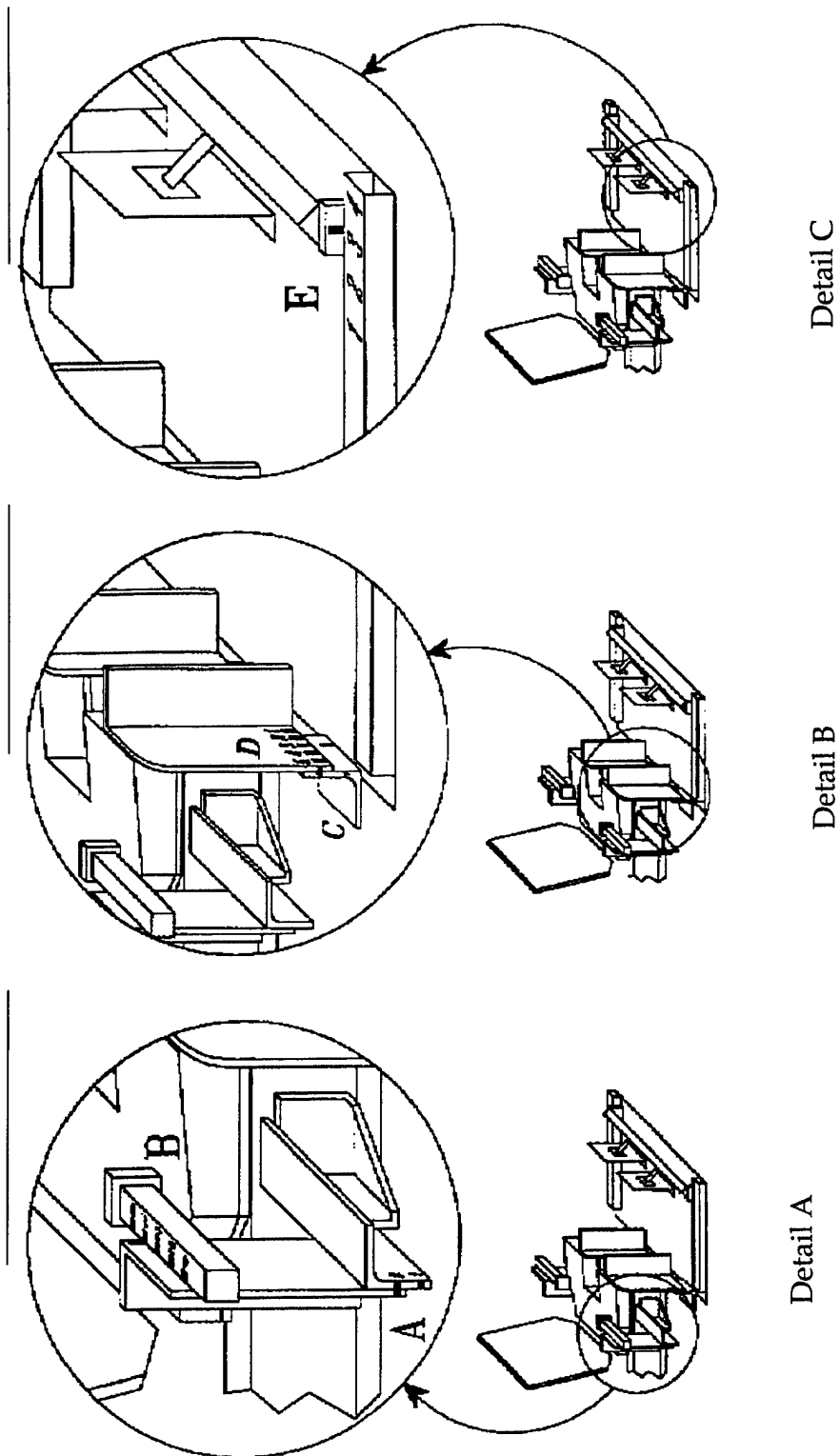


Figure A-6. Seat Adjustment Details

1.4 Transducer Calibration

Calibrations were performed before and after testing to confirm the accuracy and functional characteristics of the transducers. Pre-program and post-program calibrations are given in the Instrumentation tables at the end of this report.

The Precision Measurement Equipment Laboratories (PMEL) at Wright-Patterson Air Force Base performed the calibration of all Strainsert load cells. PMEL calibrates these devices on a periodic basis and provides current sensitivity and linearity data.

DynCorp calibrated all of the accelerometers using the comparison method (Ensor, 1970). A laboratory standard accelerometer, calibrated on a yearly basis by Endevco with standards traceable to the National Bureau of Standards, and a test accelerometer were mounted on a shaker table. Then, a random noise generator was used to drive the shaker table. Subsequent Fourier analysis of the test accelerometer outputs yielded its frequency response and phase shift. The natural frequency and the damping factor of the test accelerometer were determined, recorded and compared to previous calibration data for that test accelerometer. Sensitivities were calculated at 40 G and 100 Hertz. The sensitivity of the test accelerometer was determined by comparing its output to the output of the standard accelerometer.

DynCorp calibrated the shoulder/lap/head tri-axial load cells. These transducers were calibrated to a laboratory standard load cell in a special test fixture. The sensitivity and linearity of each test load cell were obtained by comparing the output of the test load cell to the output of the laboratory standard under identical loading conditions. The laboratory standard load cell, in turn, is calibrated by PMEL on a periodic basis.

DynCorp periodically calibrates the velocity wheel by rotating the wheel at approximately 2000, 4000 and 6000 revolutions per minute (RPM) and recording both the output voltage and the RPM.

Data Acquisition

1.5 EME DAS-64 Data Acquisition and Storage System

The EME DAS-64 Data Acquisition and Storage System was used on the Horizontal Impulse Accelerator for all tests. It is a ruggedized signal conditioning and recording system for transducers and events. The system is powered by an external 19 Volt DC power supply and communicates with the host computer through an RS-422 interface.

It is designed to withstand a 60 G, 100 ms shock from a half sine shock profile in the three primary axes. It will also withstand a 60-G amplitude, with a 10 to 2000 Hz sine sweep.

The EME DAS-64 will accommodate up to 64 transducer channels and 16 events. The signal conditioning front end excites, amplifies and offsets transducer input signals to appropriate levels for analog to digital conversion. Transducer signals are amplified, filtered, digitized and recorded in the 4 Mbyte of onboard solid-state memory. The DAS was configured to collect data at 10K samples per second. At this sample rate it can hold 129,000 samples per channel. In post processing, the sample files are decimated to 1K samples per second and filtered to cut off frequencies above 120 HZ.

The C program ADASEME on a desktop PC configured the DAS-64 prior to the start of the test, transferred test data from the EME DAS-64 when the test is completed, and stored the collected test data in a binary data file. The program communicated with the EME DAS-64 Data Acquisition System by sending instructions over the RS-422 interface.

Test data could be reviewed after it was converted to digital format using the "quick look" SCAN_EME routine. SCAN_EME produced a plot of the data stored for each channel as a function of time. The routine determined the minimum and maximum values of each data plot. It also calculated the rise time, pulse duration, and carriage acceleration, and created a disk file containing significant test parameters.

1.6 SELSPOT Motion Analysis

The Selspot Motion Analysis System utilizes photosensitive cameras to track the motion of infrared LED targets attached to different points on the test fixture. The three-dimensional motion of the LEDs was determined by combining the images from two different Selspot cameras.

For this study, two Selspot cameras were mounted onboard the sled. They were mounted with a left oblique camera and a right head-on camera. Both cameras used 24 mm lenses.

The Selspot System includes a video monitor, a desktop PC, a HW VCU-2 VME Control Unit II, and a camera interface module (MCIM). The Selspot data collection and processing are performed by the Selspot MULTILAB System software. The Selspot test data is transferred over the network to the optical disk drive on the DEC Alpha computer for permanent storage.

The Selspot System was calibrated by determining the camera locations and orientations prior to the start of the test program. The camera locations and orientations were referenced to the coordinate system of the Position Reference Structure (PRS). The PRS is shaped as a tetrahedron with reference LEDs 1, 2, 3 and 4 located at the vertices. The PRS is shown in Figure A-7.

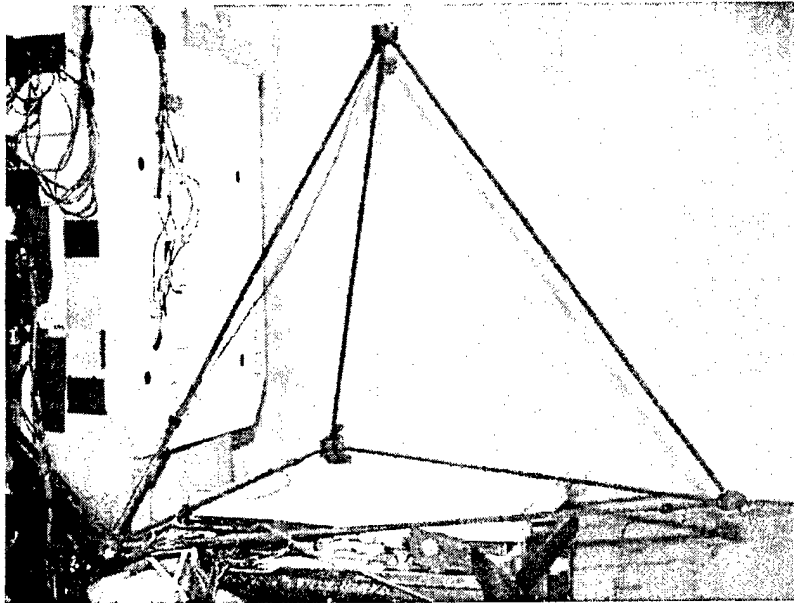
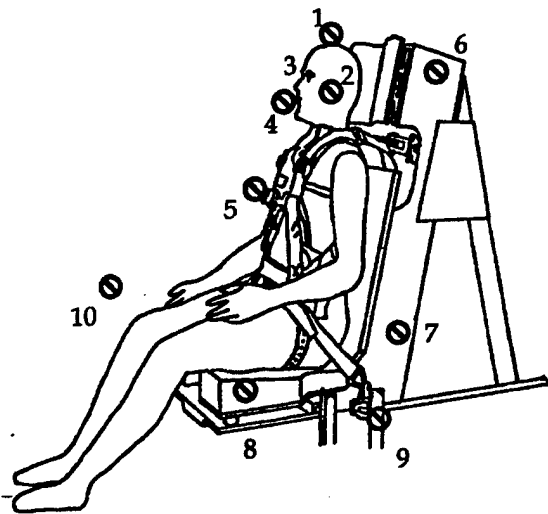


Figure A-7. SELSPOT Position Reference Structure

For all axes of the test, the motion of the subjects' helmet top, mouth, left and right ears, and chest were quantified by tracking the motion of six subject-mounted LEDs. Four reference LEDs were placed on the test fixture. Figure A-8 identifies the LED target locations.



Number	Target Name
1	Helmet Top
2	Left Helmet Ear
3	Right Helmet Ear
4	Mouth
5	Chest
6	Upper Frame
7	Lower Frame
8	Fore Seat Pan
9	Sled Mount
10	Sled Mount

Figure A-8. Selspot Target Locations

The locations of the LEDs generally followed the guidelines provided in "Film Analysis Guides for Dynamic Studies of Test Subjects, Recommended Practice (SAE J138, March 1980)."

Photogrammetric data was collected from the six moving and four reference LEDs at a 500 Hz sample rate during the impact. Five seconds of data was collected beginning at $T = -2$. The photogrammetric data was copied to an optical disk for permanent storage.

The data was processed starting at the reference mark time for 600 milliseconds on the Selspot Motion Analysis System. The camera image coordinates were corrected for camera vibration, converted into three-dimensional coordinates, and transformed into the seat coordinate seat. The processed data is stored in an MS Excel spreadsheet.

1.7 KODAK High Speed Video

A Kodak Ektapro 1000 video system was also used to provide onboard coverage of each test with nominal G levels of 20 G or less. The Kodak camera was mounted off board for tests with nominal G levels greater than 20 G. This video recorder and display unit is capable of recording high-speed motion up to a rate of 1000 frames per second. Immediate replay of the impact is possible in various rates of slow motion.

Data Processing

The Excel 97 Workbook VwhgyHac.xls is used to analyze the EME DAS test data from the VWHGY Study (Horizontal Impact Accelerator Facility). VwhgyHac.xls contains the Visual Basic module Module1 and the forms UserForm1 and UserForm2. Module1 contains one main subroutine that calls numerous other subroutines and functions. VwhgyHac.xls calls the DLL functions in the Dynamic Link Libraries Scandll and Mathdll. The shortcut ctrl+r can be used to execute the Visual Basic module. The Visual Basic module displays the two user forms.

UserForm1 requests the user to enter the system acronym, study description, impact channel number, magnitude of the impact start level, start time, processing time, T0 bit number and reference mark bit number. The user has the option to find the Kodak start time, start at the reference mark time, and use the processing time as the impact window time. The user has the option to plot the channels, print out the summary sheet, print out the plots, create a test summary file for the Biodynamic Data Bank, and create a time history file for the Biodynamic Data Bank. Default values are displayed based on the last test that was analyzed. The default values are stored in worksheet "Defaults" inside the workbook.

UserForm2 requests the user to enter the test number for each test to be processed. The default test parameters are retrieved from the test sensitivity file and displayed on the form. The user may specify new values for any of the displayed test parameters. The test parameters include the subject id, weight, age, height and sitting height. Additional parameters include the cell type, nominal g level, subject type (manikin or human) and belt preload status (computed or not computed).

The workbook contains worksheets named "Channels", "Formulas", "Preloads", "Plots", "Time History File", "Plot Pages" and "Defaults". The "Channels" worksheet contains the channel number, channel name, database ID number, channel description, and summary sheet description for each channel. The "Formulas" worksheet contains Excel formulas and Excel functions. The "Preloads" worksheet contains the preload numbers and descriptions. The "Plots" worksheet contains the channel name, the plot description, and the plot vertical axis minimum, maximum and increment for each channel to be plotted. The "Time History File" worksheet defines the channel names for the time history files (the database time history files do not use this worksheet). The "Plot Pages" worksheet allows the user to print out selected plot pages (by default, all plot pages are printed).

VwhgyHac generates time histories for the sled x, y and z axis accelerations; the sled velocity; the seat x, y and z axis accelerations; the head x, y, z, Ry, Rz and resultant accelerations; the chest x, y, z and resultant accelerations; the corrected chest x, z and resultant accelerations; the headrest x, y, tare corrected y, z, resultant and tare corrected resultant forces; the left and right shoulder x, y, z and resultant forces; the left and right lap x, y, z and resultant forces; the left and right seat pan x axis forces and their sum; the seat pan y and tare corrected y force; the left, right and center seat pan z axis forces and their sum; the seat pan resultant force; and the tare corrected seat pan resultant force.

If the test subject is human, time histories are also generated for the T1 x and y axis accelerations. If the test subject is the ADAM manikin, time histories are generated for the internal neck x, y, z and resultant forces; and the internal neck Mx, My, Mz and resultant torques.

Values for the preimpact level and the extrema for each time history are stored in the Excel worksheet summary file and printed out as a summary sheet for each test. The time histories are also plotted with up to six plots per page.

Table A-3. Sensor Setup and Calibration Log

PROGRAM: EFFECTS OF VARIABLE HELMET WEIGHT ON HUMAN RESPONSE TO +GY IMPACT (LARGE ADAM AND HUMAN)												
TEST DATES: 3 AUG 1998 – FEB 1999												
TEST NUMBERS: 6657-6995												
SAMPLE RATE: 1K												
FACILITY: HORIZONTAL ACCELERATOR												
FILTER FREQUENCY: 120 Hz												
TRANSDUCER RANGE (VOLTS): ±2.5												
DATA COLLECTION SYSTEM: EME												
DATA CHANNEL	DATA POINT	TRANSDUCER MFG. & MODEL	SERIAL NUMBER	PRE-CAL		POST-CAL		% Δ	EXC. VOL.	AMP GAIN	FULL SCALE	NOTES
				DATE	SENS	DATE	SENS					
1	SLED X ACCEL (G)	ENDEVCO 2262A-200	FR31	27-Jul-98	5.106 mv/g	19-Feb-99	5.1342 mv/g	.6	10 V	24.5	20 G	
2	SLED Y ACCEL (G)	ENTRAN EGE-72B-200	93C93C19-R07	28-Jul-98	2.3939 mv/g	19-Feb-99	2.4052 mv/g	.5	10 V	52.2	20 G	
3	SLED Z ACCEL (G)	ENTRAN EGE-72B-200	93C93C19-R02	28-Jul-98	2.2384 mv/g	19-Feb-99	2.2483 mv/g	.4	10 V	55.8	20 G	
4	SEAT PAN X ACCEL (G)	ENDEVCO 7264-200	CL83H	28-Jul-98	2.9383 mv/g	19-Feb-99	2.9312 mv/g	-.2	10V	85.1	10 G	
5	SEAT PAN Y ACCEL (G)	ENDEVCO 7264-200	CM11H	28-Jul-98	2.5707 mv/g	19-Feb-99	2.5494 mv/g	-.8	10 V	48.6	20 G	
6	SEAT PAN Z ACCEL (G)	ENDEVCO 7264-200	CM18H	28-Jul-98	3.2352 mv/g	19-Feb-99	3.2282 mv/g	-.2	10 V	77.3	10 G	
7	HEAD X ACCEL (G)	ENTRAN EGE-72B-200	93C93C19-R08	25-Nov-97	2.22 mv/g	16-Feb-99	2.2157 mv/g	-.2	10 V	56.3	20 G	
7	INT HEAD X ACCEL(G)	ENTRAN EGE-72B-200	95H95H14-A04	28-Jul-98	2.6781 mv/g	7-Aug-98	2.6739 mv/g	-.2	10 V	46.7	20 G	Manikin test 6657-6681
8	HEAD Y ACCEL (G)	ENTRAN EGE-72B-200	93C93C19-R09	25-Nov-97	2.3373 mv/g	16-Feb-99	2.3345 mv/g	-.1	10 V	35.7	30 G	
8	INT HEAD Y ACCEL(G)	ENTRAN EGE-72B-200	95H95H14-A05	28-Jul-98	-2.8421 mv/g	10-Aug-98	2.8535 mv/g	.4	10 V	29.3	30 G	Manikin test 6657-6681
9	HEAD Z ACCEL (G)	ENTRAN EGE-72B-200	93C93C19-R10	25-Nov-98	2.2186 mv/g	16-Feb-99	2.2016 mv/g	-.8	10 V	56.3	20 G	
9	INT HEAD Z ACCEL (G)	ENTRAN EGE-72B-200	93C93C19-R14	28-Jul-98	2.3034	10-Aug-98	2.3048 mv/g	.1	10 V	54.3	20 G	Manikin test 6657-6681

DATA CHANNEL	DATA POINT	TRANSDUCER MFG. & MODEL	SERIAL NUMBER	PRE-CAL		POST-CAL		EXC. VOL.	AMP GAIN	FULL SCALE	NOTES
				DATE	SENS	DATE	SENS				
10	HEAD RY ANG ACCEL (RAD/SEC2)	ENDEVCO 7302	A02Y	28-Jul-98	3.39 $\mu\text{V}/\text{rad}/\text{sec}^2$	16-Feb-99	3.39 $\mu\text{V}/\text{rad}/\text{sec}^2$	0	368.7	2000 RAD/SEC2	
11	HEAD RZ ANG ACCEL (RAD/SEC2)	ENDEVCO 7302B	PT47	28-Jul-98	3.7 $\mu\text{V}/\text{rad}/\text{sec}^2$	16-Feb-99	3.674 $\mu\text{V}/\text{rad}/\text{sec}^2$	-7	337.8	2000 RAD/SEC2	
12	CHEST X ACCEL (G)	ENTRAN EGE-72B-200	93C93C19-R11	26-Nov-97	2.249 mv/g	16-Feb-99	2.2468 mv/g	-1	55.6	20 G	
12	INT CHEST X ACCEL (G)	ENTRAN EGE-72B-200	95D95C10-G01	28-Jul-98	2.7036 mv/g	10-Aug-98	2.7205 mv/g	.6	46.2	20 G	Manikin test 6657-6681
13	CHEST Y ACCEL (G)	ENTRAN EGE-72B-200	93C93C19-R12	26-Nov-97	2.3366 mv/g	16-Feb-98	2.3289 mv/g	-3	42.8	25 G	
13	INT CHEST Y ACCEL (G)	ENTRAN EGE-72B-200	95D95C10-G02	28-Jul-98	-2.7290 mv/g	10-Aug-98	2.7361 mv/g	.3	36.6	25 G	Manikin test 6657-6681 USE NEGATIVE SENSITIVITY
14	CHEST Z ACCEL (G)	ENTRAN EGE-72B-200	93C93C19-R13	26-Nov-97	2.3741 mv/g	16-Feb-99	2.3628 mv/g	-5	52.7	20 G	
14	INT CHEST Z ACCEL (G)	ENTRAN EGE-72B-200	95D95C10-G03	28-Jul-98	2.4985 mv/g	10-Aug-98	2.5098 mv/g	.5	50	20 G	Manikin test 6657-6681
15	T1 X ACCEL (G)	ENTRAN EGAX-250	89A88L08-P09	4-Mar-98	-.6561 mv/g					20 G	Broke on test 6689. Replaced by 87E87D29-V14. Sensitivity .9884 mv/g, gain 126.5
15	T1 X ACCEL (G)	ENTRAN EGAXT-100	87E87D29-V14	24-Feb-98	.9884	16-Feb-99	.9813 mv/g	-7	126.5	20 G	Used on test 6690 and after
16	T1 Y ACCEL (G)	ENTRAN EGAX-250	89A88L08-P10	4-Mar-98	-.6787 mv/g				147.3	25 G	Broke on test 6689. Replaced by 87E87D29-V18. Sensitivity .9983 mv/g, gain 100.2
16	T1 Y ACCEL (G)	ENTRAN EGAXT-100	87E87D29-V18	10-Aug-98	.9983	16-Feb-99	1.0039 mv/g	.6	100.2	25 G	Used on test 6690 and after
17	HEADREST X FORCE (LB)	AAMRL/DYN 3D-SW	21	22-Dec-97	6.13 $\mu\text{V}/\text{lb}$	23-Feb-99	6.00 $\mu\text{V}/\text{lb}$	-2.1	407.8	1000 LB	
18	HEADREST Y FORCE (LB)	AAMRL/DYN 3D-SW	21	22-Dec-97	-4.97 $\mu\text{V}/\text{lb}$	23-Feb-99	4.86 $\mu\text{V}/\text{lb}$	-2.2	503	1000 LB	USE NEGATIVE SENSITIVITY
19	HEADREST Z FORCE (LB)	AAMRL/DYN 3D-SW	21	22-Dec-97	-5.22 $\mu\text{V}/\text{lb}$	23-Feb-99	5.10 $\mu\text{V}/\text{lb}$	-2.3	478.9	1000 LB	USE NEGATIVE SENSITIVITY

DATA CHANNEL	DATA POINT	TRANSDUCER MFG. & MODEL NUMBER	PRE-CAL		POST-CAL		EXC. VOL.	AMP GAIN	FULL SCALE	NOTES
			DATE	SENS	DATE	SENS				
20	LEFT SHOULDER X FORCE (LB)	AAMRL/DYN 3D-SW	10-Sep-97	-6.16 $\mu\text{v/lb}$	22-Feb-99	6.08 $\mu\text{v/lb}$	10 V	215.6	1500 LB	USE NEGATIVE SENSITIVITY
21	LEFT SHOULDER Y FORCE (LB)	AAMRL/DYN 3D-SW	10-Sep-97	-5.24 $\mu\text{v/lb}$	22-Feb-99	5.11 $\mu\text{v/lb}$	10 V	175.3	2000 LB	USE NEGATIVE SENSITIVITY
22	LEFT SHOULDER Z FORCE (LB)	AAMRL/DYN 3D-SW	10-Sep-97	-4.82 $\mu\text{v/lb}$	22-Feb-99	4.69 $\mu\text{v/lb}$	10 V	243.3	1500 LB	USE NEGATIVE SENSITIVITY
23	RIGHT SHOULDER X FORCE (LB)	AAMRL/DYN 3D-SW	30-Mar-98	-7.49 $\mu\text{v/lb}$	23-Feb-99	7.29 $\mu\text{v/lb}$	10 V	222.5	1500 LB	USE NEGATIVE SENSITIVITY
24	RIGHT SHOULDER Y FORCE (LB)	AAMRL/DYN 3D-SW	30-Mar-98	-6.93 $\mu\text{v/lb}$	23-Feb-99	6.76 $\mu\text{v/lb}$	10 V	180.4	2000 LB	USE NEGATIVE SENSITIVITY
25	RIGHT SHOULDER Z FORCE (LB)	AAMRL/DYN 3D-SW	30-Mar-98	-6.93 $\mu\text{v/lb}$	23-Feb-99	6.76 $\mu\text{v/lb}$	10 V	243.7	1500 LB	USE NEGATIVE SENSITIVITY
26	LEFT LAP X FORCE (LB)	AAMRL/DYN 3D-SW	30-Mar-98	-7.58 $\mu\text{v/lb}$	19-Feb-99	7.36 $\mu\text{v/lb}$	10 V	219.9	1500 LB	USE NEGATIVE SENSITIVITY
27	LEFT LAP Y FORCE (LB)	AAMRL/DYN 3D-SW	30-Mar-98	-7.10 $\mu\text{v/lb}$	19-Feb-99	7.05 $\mu\text{v/lb}$	10 V	176.1	2000 LB	USE NEGATIVE SENSITIVITY
28	LEFT LAP Z FORCE (LB)	AAMRL/DYN 3D-SW	30-Mar-98	-6.77 $\mu\text{v/lb}$	19-Feb-99	6.71 $\mu\text{v/lb}$	10 V	246.2	1500 LB	USE NEGATIVE SENSITIVITY
29	RIGHT LAP X FORCE (LB)	AAMRL/DYN 3D-SW	26-Mar-98	-7.53 $\mu\text{v/lb}$	22-Feb-99	7.31 $\mu\text{v/lb}$	10 V	221.3	1500 LB	USE NEGATIVE SENSITIVITY
30	RIGHT LAP Y FORCE (LB)	AAMRL/DYN 3D-SW	26-Mar-98	7.03 $\mu\text{v/lb}$	22-Feb-99	6.85 $\mu\text{v/lb}$	10 V	177.8	2000 LB	USE NEGATIVE SENSITIVITY
31	RIGHT LAP Z FORCE (LB)	AAMRL/DYN 3D-SW	26-Mar-98	-7.35 $\mu\text{v/lb}$	22-Feb-99	7.39 $\mu\text{v/lb}$	10 V	226.8	1500 LB	USE NEGATIVE SENSITIVITY
32	LEFT SEAT PAN Z FORCE (LB)	STRAINERT FL2.5-2 SGKT	29-Apr-98	-7.9 $\mu\text{v/lb}$		Not Required	10 V	211	1500 LB	USE NEGATIVE SENSITIVITY

DATA CHANNEL	DATA POINT	TRANSDUCER MFG. & MODEL	SERIAL NUMBER	PRE-CAL		POST-CAL		EXC. VOL.	AMP GAIN	FULL SCALE	NOTES
				DATE	SENS	DATE	SENS				
33	RIGHT SEAT PAN Z FORCE (LB)	STRAINERT FL2.5- 2 SPKT	Q7135-3	30-Apr-98	-7.9 $\mu\text{v/lb}$		Not Required	10 V	211	1500 LB	USE NEGATIVE SENSITIVITY
34	CENTER SEAT PAN Z FORCE (LB)	STRAINERT FL2.5- 2 SPKT	Q7588-2	29-Apr-98	-7.85 $\mu\text{v/lb}$		Not Required	10 V	212.3	1500 LB	USE NEGATIVE SENSITIVITY
35	LEFT SEAT PAN X FORCE (LB)	AAMRL / DYN LINK	003	19-Dec-97	-10.84 $\mu\text{v/lb}$		Not Required	10 V	153.8	1500 LB	USE NEGATIVE SENSITIVITY
36	RIGHT SEAT PAN X FORCE (LB)	AAMRL / DYN LINK	5	19-Dec-97	10.05 $\mu\text{v/lb}$		Not Required	10 V	165.8	1500 LB	
37	CENTER SEAT PAN Y FORCE (LB)	AAMRL / DYN LINK	4	19-Dec-98	9.94 $\mu\text{v/lb}$		Not Required	10V	167.7	1500 LB	
38	INT HEAD RX ANG ACCEL (RAD/SEC2)	ENDEVCO 7302B	FM93	26-Nov-97	3.73 $\mu\text{v/rad/sec}^2$	11-Aug-98	3.67 $\mu\text{v/rad/sec}^2$	10 V	134	5000 RAD/SEC2	Manikin test 6657-6681
39	INT NECK X FORCE (LB)	DENTON 1716A	820	12-Jan-98	8.06 $\mu\text{v/lb}$	11-Aug-98	8.01 $\mu\text{v/lb}$	10 V	310.2	1000 LB	Manikin test 6657-6681
40	INT NECK Y FORCE (LB)	DENTON 1716A	820	12-Jan-98	8.35 $\mu\text{v/lb}$	11-Aug-98	8.16 $\mu\text{v/lb}$	10 V	299.4	1000 LB	Manikin test 6657-6681
41	INT NECK Z FORCE (LB)	DENTON 1716A	820	12-Jan-98	4.46 $\mu\text{v/lb}$	11-Aug-98	4.59 $\mu\text{v/lb}$	10 V	560.4	1000 LB	Manikin test 6657-6681
42	INT NECK MX TORQUE (IN- LB)	DENTON 1716A	820	12-Jan-98	-6.70 $\mu\text{v/lb}$	11-Aug-98	6.7 $\mu\text{v/lb}$	10 V	373.1	1000 IN-LB	Manikin test 6657-6681 USE NEGATIVE SENSITIVITY
43	INT NECK MY TORQUE (IN- LB)	DENTON 1716A	820	12-Jan-98	6.81 $\mu\text{v/lb}$	11-Aug-98	6.7 $\mu\text{v/lb}$	10 V	367.1	1000 IN-LB	Manikin test 6657-6681
44	INT NECK MZ TORQUE (IN- LB)	DENTON 1716A	820	12-Jan-98	9.15 $\mu\text{v/lb}$	11-Aug-98	9.13 $\mu\text{v/lb}$	10 V	273.2	1000 IN-LB	Manikin test 6657-6681

DATA CHANNEL	DATA POINT	TRANSDUCER MFG. & MODEL	SERIAL NUMBER	PRE-CAL		POST-CAL		% Δ	EXC. VOL.	AMP GAIN	FULL SCALE	NOTES
				DATE	SENS	DATE	SENS					
45	SLED VELOCITY (FT/SEC)	GLOBE 22A672-2	2		21.82 mv/ft				10 V	2	57.28 FT/SEC	Raw Sensitivity=.1523 v/rev/sec; [(12 in/ft) / (10.3 in/rev) x .1523 v/r/s =.1774 v/rev/ft ; Atten @ 8.130 ; .1774 v/ft/s (1 / 8.130) = .02182 v/ft/s Replaced on test 6956; Sens 25.12 mv/ft.
45	SLED VELOCITY (FT/SEC)	GLOBE 22A672-2	5		25.12 mv/ft				10 V	2	49.76 FT/SEC	Raw Sensitivity=.1753 v/rev/sec; [(12 in/ft) / (10.3 in/rev) x .1753 v/r/s =.2042 v/rev/ft ; Atten @ 8.130 ; .2042 v/ft/s (1 / 8.130) = .02512 v/ft/s Replaced on test 6956.
D-3	REFERENCE SWITCH (VOLTS)				1 v							DIGITAL INPUT CHANNEL 3
D-4	T0 PULSE (VOLTS)				1 v							DIGITAL INPUT CHANNEL 4

APPENDIX B

Subject Anthropometry/ Instrumentation Channel Definitions

Table B-1. Human Subject Anthropometry

SUBJECT ID	SUBJECT SEX	AGE (YR)	WEIGHT (LB)	STAND HT. (IN)	SITTING HT. (IN)
B-16	F	31	130	65.3	35.2
B-22	F	29	135	68.3	36.1
B-26	F	21	146	64.1	33.8
C-19	F	27	171	66.6	35.6
E-5	F	25	140	65.7	34.5
L-11	F	32	135	64.8	33.7
M-32	F	33	122	64.1	33.4
P-12	F	30	168	64.2	33.9
S-23	F	26	164	64.3	34.1
W-11	F	21	142	63.8	34.4
B-9	M	32	155	68.1	34.9
B-11	M	37	225	72.7	37.5
B-23	M	37	189	70.9	37.2
B-24	M	32	204	69.6	38.1
B-25	M	20	152	71.9	36.3
C-12	M	35	185	68.1	36.6
C-17	M	32	175	69.5	37.9
D-11	M	32	239	70.7	38
D-12	M	29	169	67.3	36
D-13	M	35	220	73.6	38.8
E-4	M	35	208	71.5	38.4
H-13	M	35	160	71	36.4
H-16	M	42	180	67	35.7
H-18	M	27	234	72	37.5
H-19	M	20	204	71.5	37.2
J-7	M	30	160	67.7	35.6
M-21	M	39	150	66.1	34.2
R-21	M	38	228	71.3	38.1
S-11	M	32	219	71.2	37
W-12	M	43	183	68.3	35.1
Y-4	M	28	194	69.4	35.7
MEAN		31.1	177	68.4	36
STD DEV		6	33.5	2.96	1.6
USAF MEAN		30	173.6	69.8	36.7
STD DEV		6.3	21.4	2.4	1.3

Table B-2. Electronic Data Channel List

Channel No.	Parameter	Dynamic Range	Frequency Range
1	Sled X Accel.	20 G	DC – 120 Hz
2	Seat Pan X Accel.	10 G	DC – 120 Hz
3	Seat Pan Y Accel.	20 G	DC – 120 Hz
4	Seat Pan Z Accel.	10 G	DC – 120 Hz
5	Head X Accel.	20 G	DC – 120 Hz
6	Head Y Accel.	30 G	DC – 120 Hz
7	Head Z Accel.	20 G	DC – 120 Hz
8	Head Ry Ang. Accel.	2000 Rad/Sec ²	DC – 120 Hz
9	Head Rz Ang. Accel.	2000 Rad/Sec ²	DC – 120 Hz
10	Chest X Accel.	20 G	DC – 120 Hz
11	Chest Y Accel.	25 G	DC – 120 Hz
12	Chest Z Accel.	20 G	DC – 120 Hz
13	T1 X Accel.	20 G	DC – 120 Hz
14	T1 Y Accel.	25 G	DC – 120 Hz
15	Head Rest X Force	500 lb	DC – 120 Hz
16	Head Rest Y Force	500 lb	DC – 120 Hz
17	Head Rest Z Force	500 lb	DC – 120 Hz
18	Left Shoulder X Force	1500 lb	DC – 120 Hz
19	Left Shoulder Y Force	2000 lb	DC – 120 Hz
20	Left Shoulder Z Force	1500 lb	DC – 120 Hz
21	Right Shoulder X Force	1500 lb	DC – 120 Hz
22	Right Shoulder Y Force	2000 lb	DC – 120 Hz
23	Right Shoulder Z Force	1500 lb	DC – 120 Hz
24	Left Lap X Force	1500 lb	DC – 120 Hz
25	Left Lap Y Force	2000 lb	DC – 120 Hz
26	Left Lap Z Force	1500 lb	DC – 120 Hz
27	Right Lap X Force	1500 lb	DC – 120 Hz
28	Right Lap Y Force	2000 lb	DC – 120 Hz
29	Right Lap Z Force	1500 lb	DC – 120 Hz
30	Left Seat Pan X Force	1500 lb	DC – 120 Hz
31	Left Seat Pan Z Force	1500 lb	DC – 120 Hz
32	Center Seat Pan Y Force	1500 lb	DC – 120 Hz
33	Center Seat Pan Z Force	1500 lb	DC – 120 Hz
34	Right Seat Pan X Force	1500 lb	DC – 120 Hz

Table B-3. Additional Electronic Data Channels: ADAM Tests

Channel No.	Parameter	Dynamic Range	Frequency Range
35	Right Seat Pan Z Force	1500 lb	DC – 120 Hz
36	Event		DC – 2000 Hz
37	Int. Head X Accel.	25 G	DC – 120 Hz
38	Int. Head Y Accel.	35 G	DC – 120 Hz
39	Int. Head Z Accel.	25 G	DC – 120 Hz
40	Int. Head Rx Ang. Accel.	5000 Rad/Sec ²	DC – 120 Hz
41	Int. Head Ry Ang. Accel.	5000 Rad/Sec ²	DC – 120 Hz
42	Int. Head Rz Ang. Accel.	5000 Rad/Sec ²	DC – 120 Hz
43	Int. Neck X Force	500 lb	DC – 120 Hz
44	Int. Neck Y Force	1000 lb	DC – 120 Hz
45	Int. Neck Z Force	500 lb	DC – 120 Hz
46	Int. Neck Mx Torque	500 in-lb	DC – 120 Hz
47	Int. Neck My Torque	1000 in-lb	DC – 120 Hz
48	Int. Neck Mz Torque	500 in-lb	DC – 120 Hz
49	Int. Chest X Accel.	30 G	DC – 120 Hz
50	Int. Chest Y Accel.	40 G	DC – 120 Hz
51	Int. Chest Z Accel.	30 G	DC – 120 Hz

APPENDIX C

Sample Acceleration/Force Data

VWHGY Study Test: 6810 Test Date: 981016 Subj: M-32 Wt: 128.0

Nom G: 6.0 Cell: C

Data ID	Immediate Preimpact	Maximum Value	Minimum Value	Time Of Maximum	Time Of Minimum
Kodak Start Time (Ms)				-2185.0	
Reference Mark Time (Ms)				-135.0	
Impact Rise Time (Ms)				74.0	
Impact Duration (Ms)				140.0	
Velocity Change (Ft/Sec)		17.47			
Sled Acceleration (G)					
X Axis	0.03	5.95	-0.51	74.0	147.0
Y Axis	0.00	1.24	-0.51	65.0	73.0
Z Axis	1.00	1.81	0.48	21.0	40.0
Sled Velocity (Ft/Sec)	0.06	17.63	0.09	151.0	0.0
Seat Pan Acceleration (G)					
X Axis	0.00	0.68	-1.50	72.0	65.0
Y Axis	0.02	6.64	-2.16	65.0	192.0
Z Axis	1.00	1.53	-2.04	81.0	192.0
Head Acceleration (G)					
X Axis	0.03	2.35	-6.25	199.0	132.0
Y Axis	0.05	11.03	-0.64	144.0	183.0
Z Axis	1.01	2.60	-4.61	162.0	130.0
Resultant	1.02	12.11	0.49	143.0	186.0
Head Angular Accel (Rad/Sec2)					
Ry Axis	-4.12	260.85	-336.86	200.0	162.0
Rz Axis	-6.74	330.10	-580.16	183.0	152.0
Chest Acceleration (G)					
X Axis	-0.01	1.86	-1.55	153.0	185.0
Y Axis	-0.01	9.48	-0.72	113.0	190.0
Z Axis	1.00	2.86	-0.48	91.0	148.0
Resultant	1.00	9.51	0.34	113.0	36.0
Corrected Chest Acceleration (G)					
X Axis	-0.01	2.10	-1.59	153.0	183.0
Z Axis	1.00	2.76	-0.16	91.0	145.0
Resultant	1.00	9.50	0.18	113.0	35.0
T1 Acceleration (G)					
X Axis	-0.01	1.84	-2.00	174.0	89.0
Y Axis	0.00	9.47	-1.71	95.0	168.0

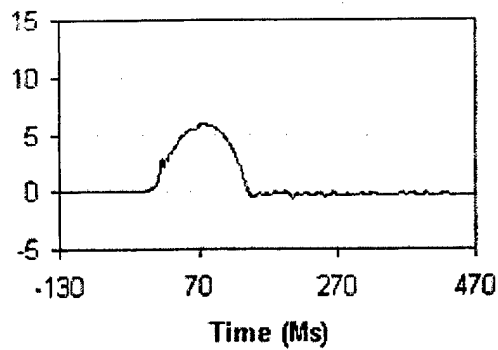
VWHGY Study Test: 6810 Test Date: 981016 Subj: M-32 Wt: 128.0
 Nom G: 6.0 Cell: C

Data ID	Immediate Preimpact	Maximum Value	Minimum Value	Time Of Maximum	Time Of Minimum
Headrest Force (Lb)					
X Axis	20.63	63.33	-6.98	194.0	162.0
Y Axis	-9.75	91.56	-43.21	81.0	196.0
Y Axis Minus Tare	-9.87	65.01	-42.72	81.0	196.0
Z Axis	-6.45	5.76	-25.00	191.0	90.0
Resultant	23.71	104.38	5.44	80.0	142.0
Resultant Minus Tare	23.76	82.36	5.28	80.0	121.0
Left Shoulder Force (Lb)					
X Axis	8.35	25.92	5.42	119.0	23.0
Y Axis	-11.33	63.88	-11.33	120.0	0.0
Z Axis	59.91	149.99	53.32	116.0	19.0
Resultant	61.54	164.59	54.24	118.0	20.0
Right Shoulder Force (Lb)					
X Axis	-63.74	-34.87	-146.20	200.0	122.0
Y Axis	-18.40	75.67	-18.06	123.0	0.0
Z Axis	18.19	49.66	8.64	121.0	45.0
Resultant	68.80	171.95	41.66	123.0	45.0
Left Lap Force (Lb)					
X Axis	-61.54	-49.65	-128.01	200.0	111.0
Y Axis	28.70	170.27	11.13	108.0	200.0
Z Axis	-99.97	-72.14	-280.87	200.0	115.0
Resultant	120.85	350.64	88.28	115.0	200.0
Right Lap Force (Lb)					
X Axis	-44.76	-39.63	-88.71	200.0	111.0
Y Axis	-46.82	-1.56	-51.37	88.0	187.0
Z Axis	-87.00	-69.42	-143.38	200.0	114.0
Resultant	108.46	169.13	91.19	114.0	40.0

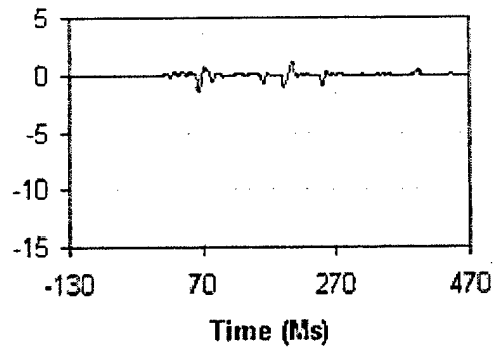
VWHGY Study Test: 6810 Test Date: 981016 Subj: M-32 Wt: 128.0
 Nom G: 6.0 Cell: C

Data ID	Immediate Preimpact	Maximum Value	Minimum Value	Time Of Maximum	Time Of Minimum
Seat Pan Force (Lb)					
Left X Axis	8.19	75.78	-61.14	113.0	67.0
Right X Axis	7.77	100.80	-113.11	167.0	85.0
X Axis Sum	15.96	127.53	-150.09	167.0	85.0
Y Axis	-6.25	182.86	-88.83	106.0	196.0
Y Axis Minus Tare	-6.95	95.36	-86.06	178.0	196.0
Left Z Axis	22.19	132.04	-15.89	192.0	198.0
Right Z Axis	122.48	209.88	18.75	66.0	193.0
Center Z Axis	114.30	192.79	84.38	109.0	161.0
Z Axis Sum	258.97	388.97	183.17	82.0	195.0
Resultant	259.54	426.51	201.41	82.0	195.0
Resultant Minus Tare	259.56	417.33	200.69	82.0	195.0

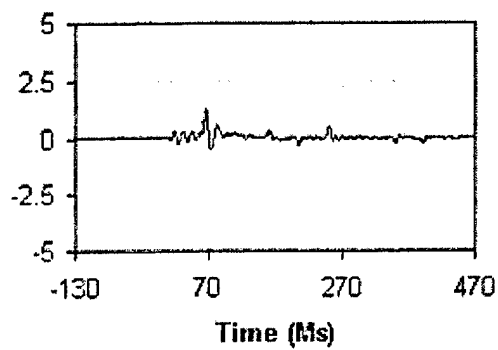
SLED X ACCEL (G)



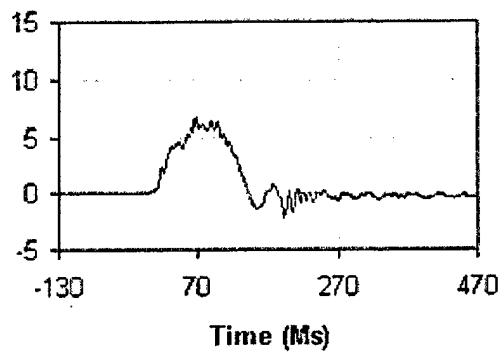
SEAT PAN X ACCEL (G)



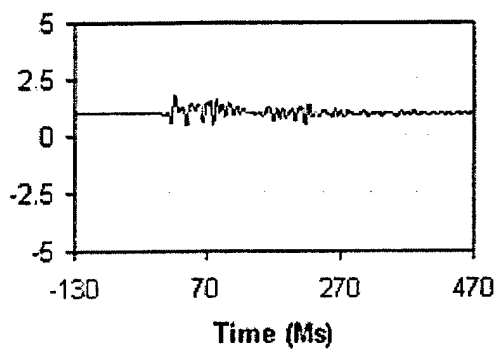
SLED Y ACCEL (G)



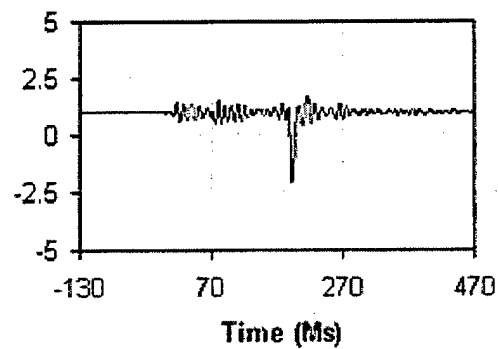
SEAT PAN Y ACCEL (G)



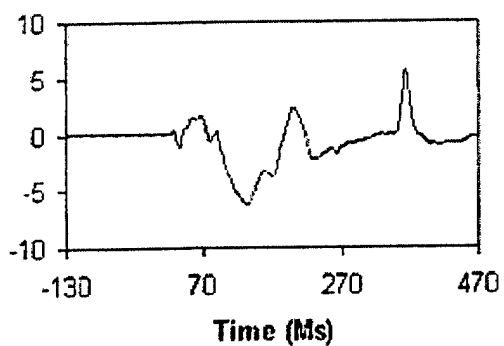
SLED Z ACCEL (G)



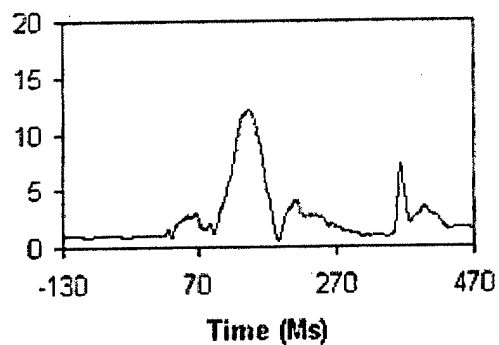
SEAT PAN Z ACCEL (G)



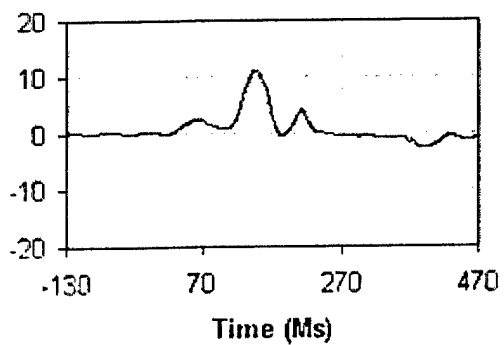
HEAD X ACCEL (G)



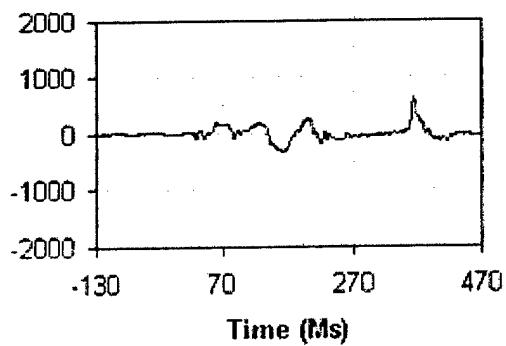
HEAD RESULTANT (G)



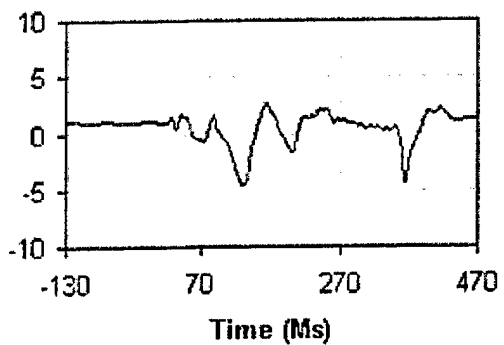
HEAD Y ACCEL (G)



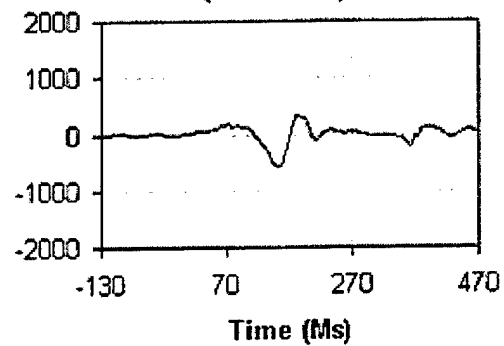
HEAD Ry ANG ACCEL (RAD/SEC²)



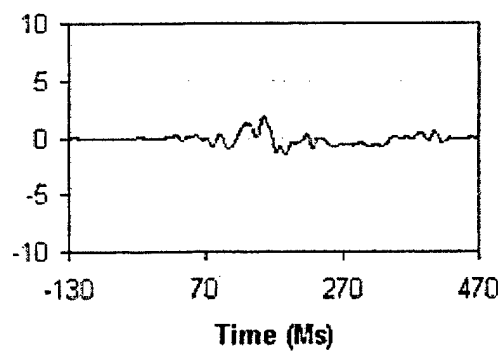
HEAD Z ACCEL (G)



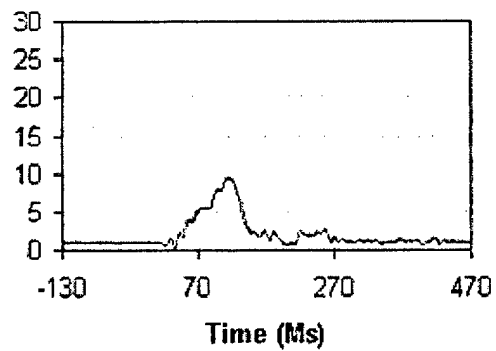
HEAD Rz ANG ACCEL (RAD/SEC²)



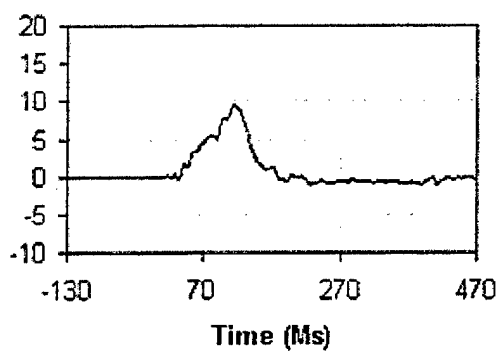
CHEST X ACCEL (G)



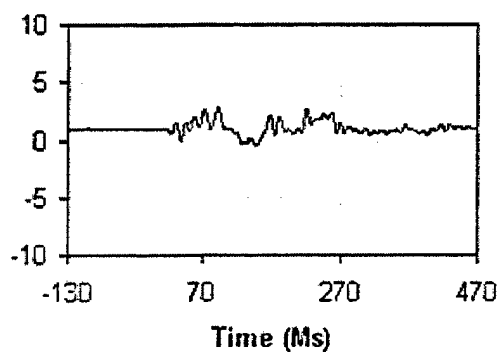
CHEST RESULTANT (G)



CHEST Y ACCEL (G)

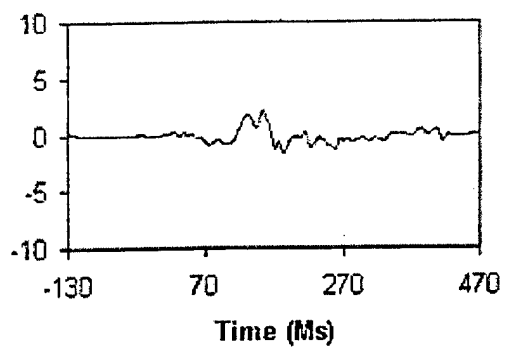


CHEST Z ACCEL (G)

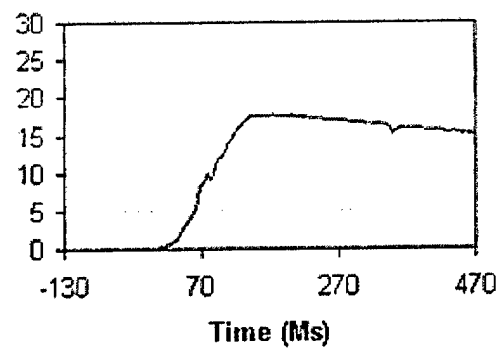


VWHGY Study Test: 6810 Test Date: 981016 Subj: M-32 Cell: C

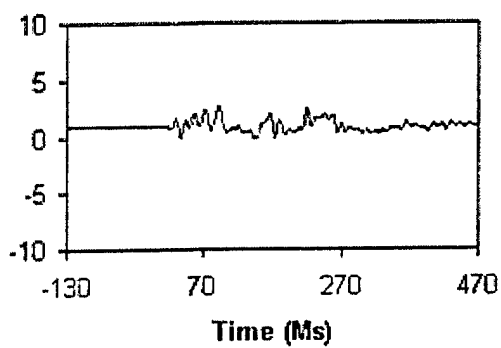
CORRECTED CHEST X ACCEL (G)



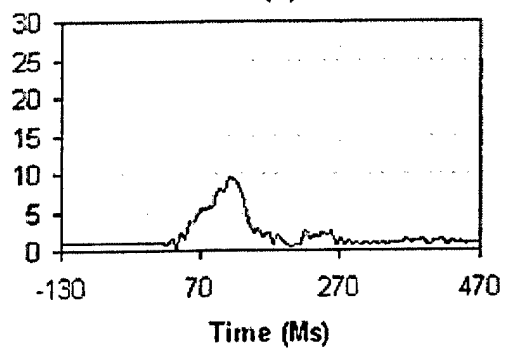
SLED VELOCITY (FT/SEC)



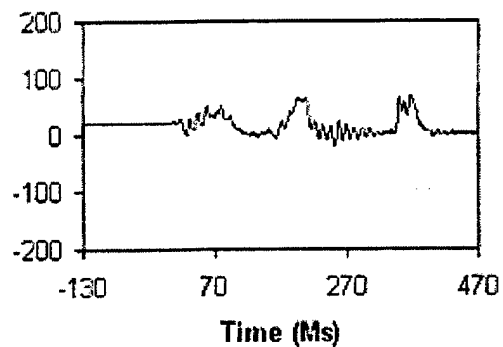
CORRECTED CHEST Z ACCEL (G)



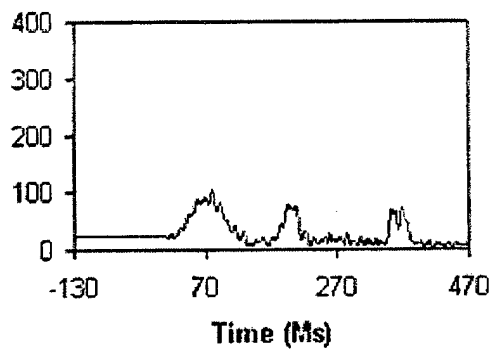
CORRECTED CHEST RESULTANT (G)



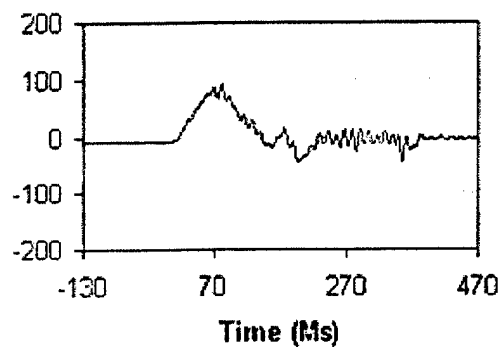
HEADREST X FORCE (LB)



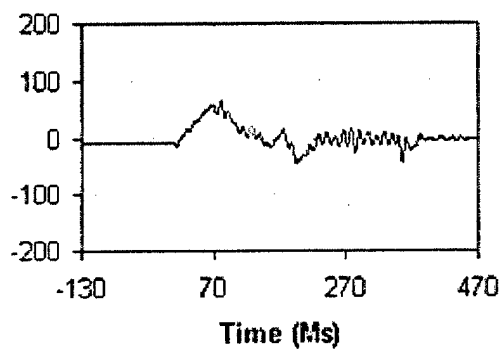
HEADREST RESULTANT (LB)



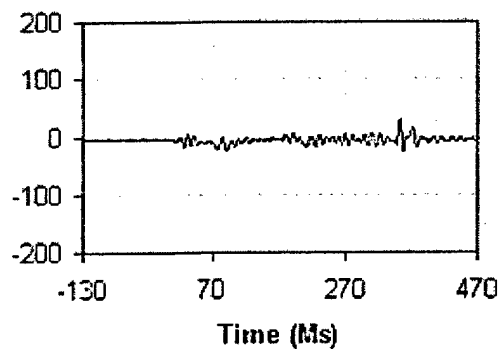
HEADREST Y FORCE (LB)



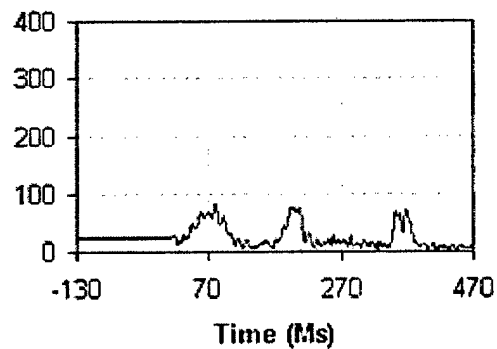
HEADREST Y MINUS TARE (LB)



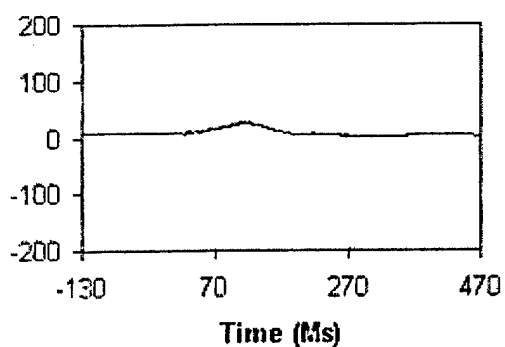
HEADREST Z FORCE (LB)



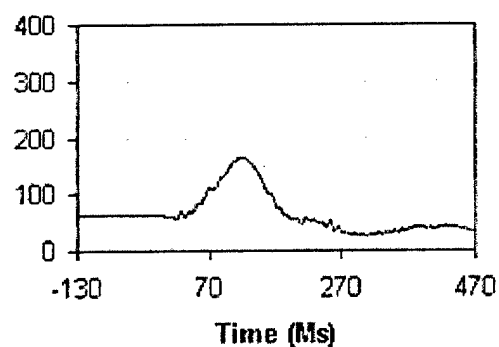
HEADREST RES MINUS TARE (LB)



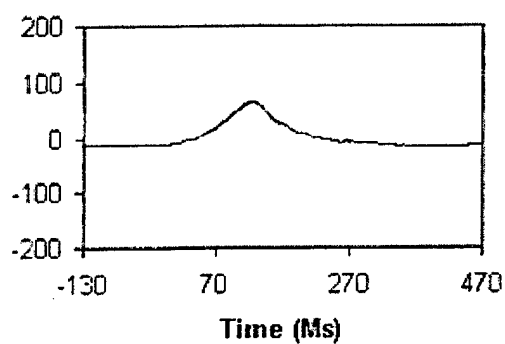
LEFT SHOULDER X FORCE (LB)



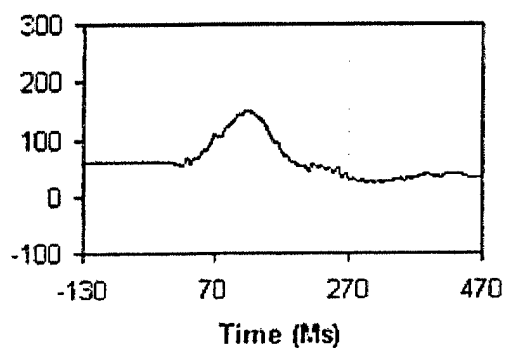
LEFT SHOULDER RESULTANT (LB)



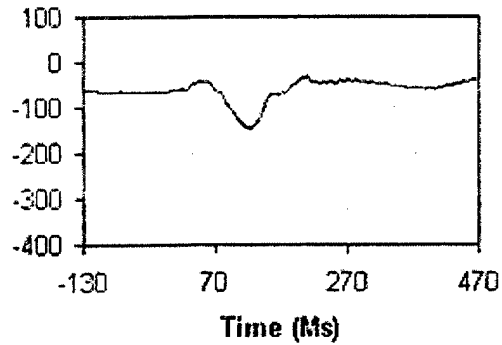
LEFT SHOULDER Y FORCE (LB)



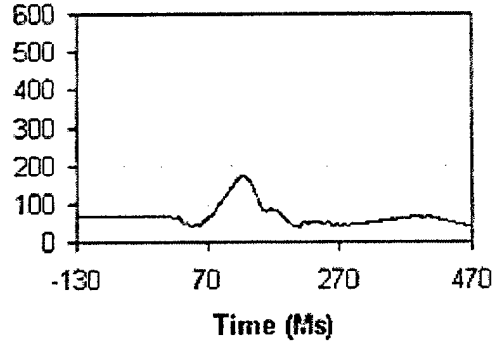
LEFT SHOULDER Z FORCE (LB)



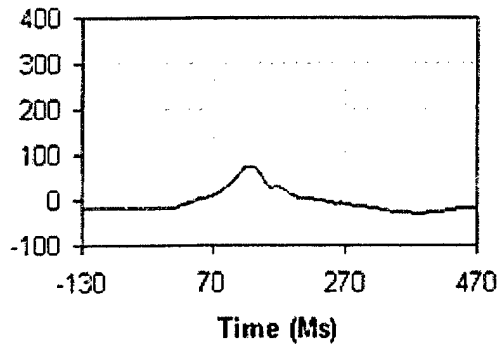
RIGHT SHOULDER X FORCE (LB)



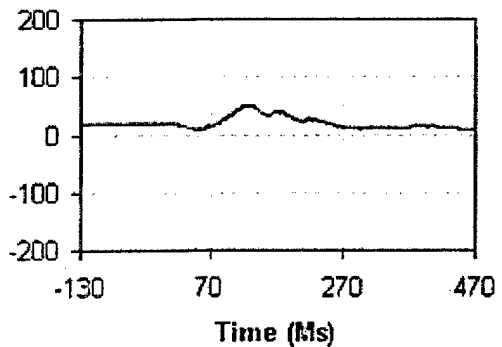
RIGHT SHOULDER RESULTANT (LB)



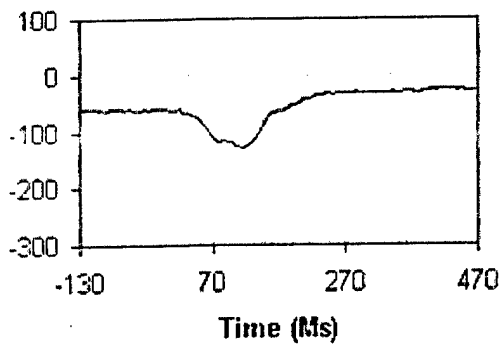
RIGHT SHOULDER Y FORCE (LB)



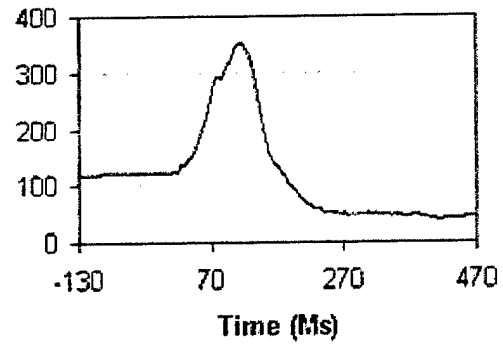
RIGHT SHOULDER Z FORCE (LB)



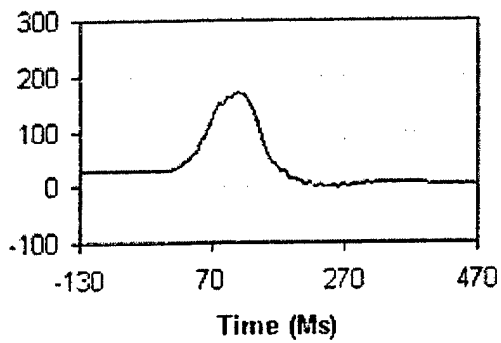
LEFT LAP X FORCE (LB)



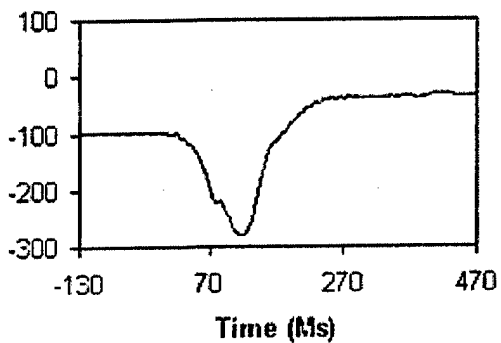
LEFT LAP RESULTANT (LB)



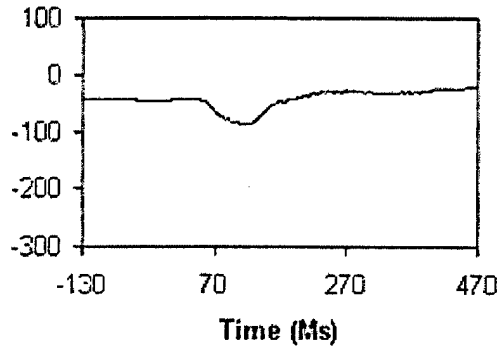
LEFT LAP Y FORCE (LB)



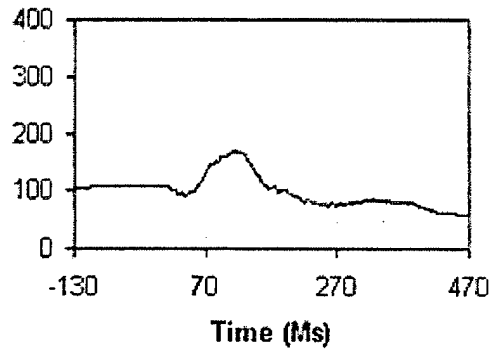
LEFT LAP Z FORCE (LB)



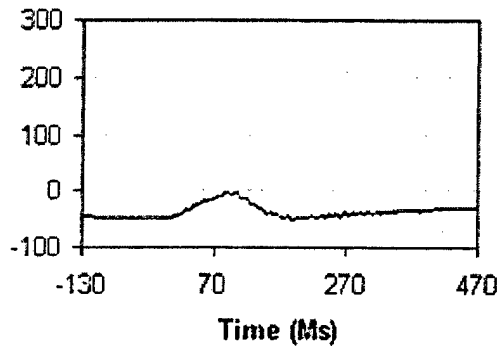
RIGHT LAP X FORCE (LB)



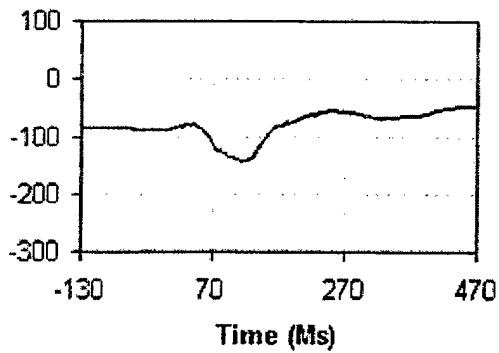
RIGHT LAP RESULTANT (LB)



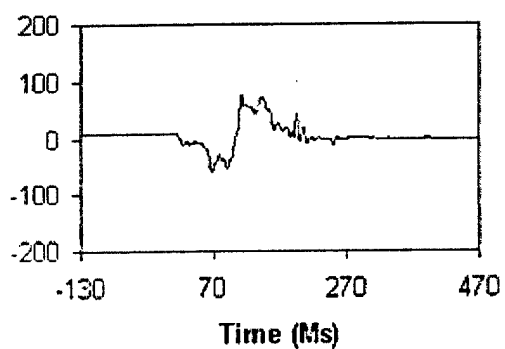
RIGHT LAP Y FORCE (LB)



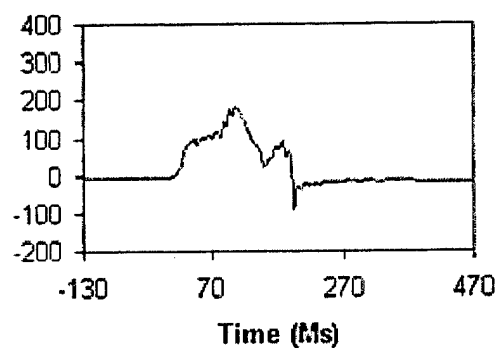
RIGHT LAP Z FORCE (LB)



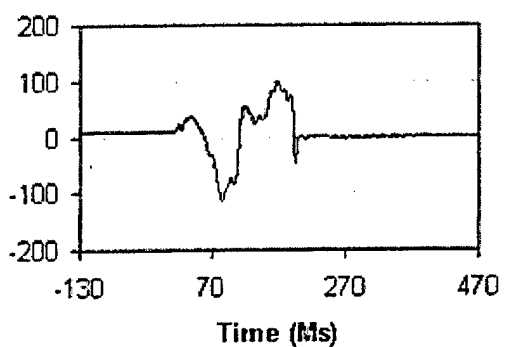
LEFT SEAT PAN X FORCE (LB)



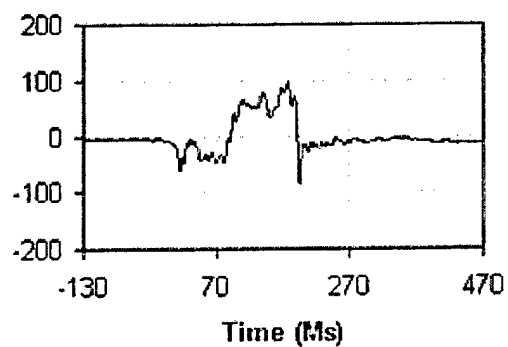
SEAT PAN Y FORCE (LB)



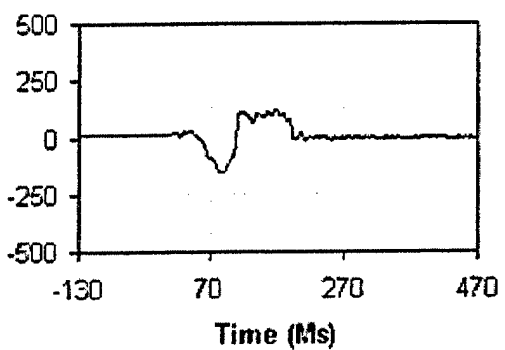
RIGHT SEAT PAN X FORCE (LB)



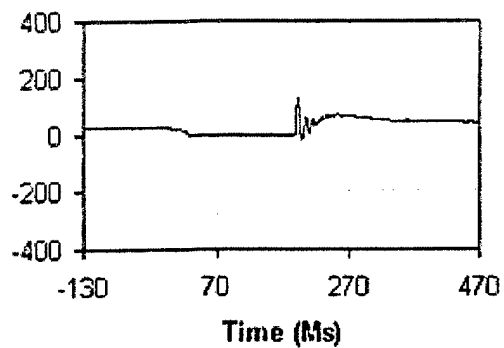
SEAT PAN Y MINUS TARE (LB)



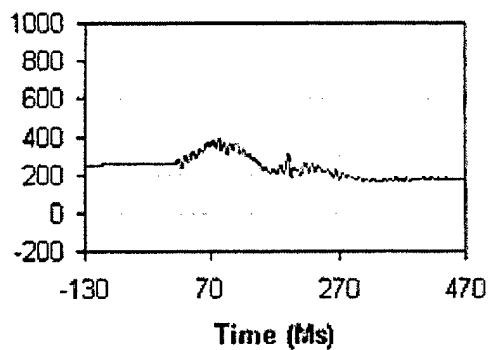
SEAT PAN X SUM (LB)



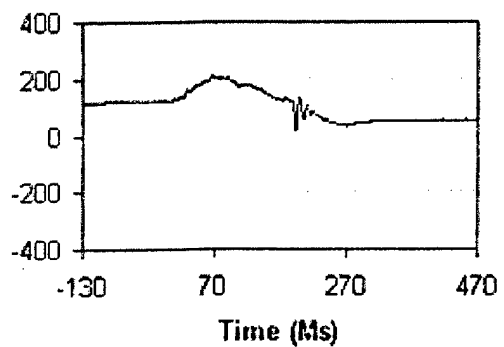
LEFT SEAT PAN Z FORCE (LB)



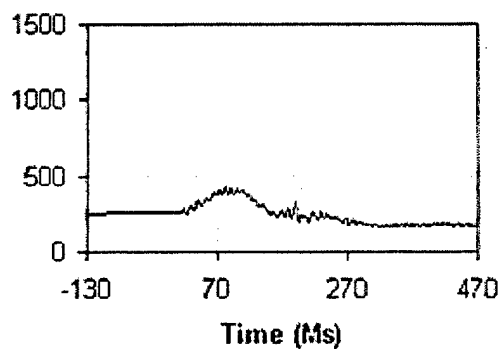
SEAT PAN Z SUM (LB)



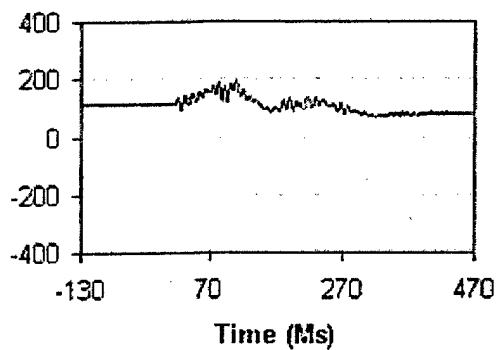
RIGHT SEAT PAN Z FORCE (LB)



SEAT PAN RESULTANT (LB)



CENTER SEAT PAN Z FORCE (LB)



SEAT PAN RES MINUS TARE (LB)

